A. R., Shipley-Phillips J. K., Everitt J. I., Tewksbury E. W., Moss O.R., Wrong B. A., Dodd D. F., Andersen M. E., Bonner J. C., *Nat. Nanotechnol.*, **4**, 747–751 (2009).

12) Shvedova A. A., Kishin E. R., Mercer R., Murray A. R., Johnson V. J., Potapovich A. I., Tyurina Y. Y., Gorelik O., Arepalli S., Schwegler-Berry D., Hubbs A. F., Antonini J., Evans D. E., Ku B. K., Ramsey D., Maynard A., Kagan V. E., Castranova V., Baron P., *Am. J. Physiol. Lung cell. mol. physiol.*, **289**, L698–L708 (2005).

13) Li Z., Hulderman T., Salmen R., Chapman R., Leonars S. S., Young S. H., Shvedova A., Luster M. I., Simeonove P. P., *Environ. Health Perspect.*, **115**, 377–382 (2007).

14) Nemmar A., Hoet P. H., Vandervoort P., Dinsdale D., Nemery B., Hoylaerts M. F., *J. Thromb. Haemost.*, **5**, 1217–1226 (2007).

15) Park E. J., Cho W. S., Jeong J., Yi J., Choi K., Park K., *Toxicology*, **259**, 113–121 (2009).

16) Nygaard U. C., Hansen J. S., Samuelsen M., Alberg T., Marioara C. D., Løvik M., *Toxicol. Sci.*, **109**, 113–123 (2009).

17) Inoue K., Koike E., Yanagisawa R., Hirano S., Nishikwa M., Takano H., *Toxicol. Appl. Pharmacol.*, **237**, 306–316 (2009).

Genes and Environment, Vol. 33, No. 1 pp. 27-31 (2011)

Short communication

Fullerene (C_{60}) Is Negative in the *In Vivo Pig-A* Gene Mutation Assay

Katsuyoshi Horibata[1,5], Akiko Ukai[1], Naoki Koyama[1], Atsuya Takagi[2], Jun Kanno[2], Takafumi Kimoto[3], Daishiro Miura[3], Akihiko Hirose[4] and Masamitsu Honma[1]

[1]Division of Genetics and Mutagenesis, National Institute of Health Sciences, Tokyo, Japan
[2]Division of Toxicology, National Institute of Health Sciences, Tokyo, Japan
[3]TEIJIN Pharma Limited, Tokyo, Japan
[4]Division of Risk Assessment, National Institute of Health Sciences, Tokyo, Japan

(Received December 24, 2010; Revised January 20, 2011; accepted January 21, 2011)

Carbon nanoparticles, such as carbon nanotubes and fullerene (C_{60}), are potential candidates as leading substances in nanotechnological fields, but little is known about their safety. Here we examined *in vivo* genotoxicity of C_{60}, by performing the *Pig-A* gene mutation assay in the peripheral blood of male C57BL/6Cr mice. Mice were given single intraperitoneal injection of 3 mg of C_{60} particles in 0.5 mL suspension containing 0.1%-Tween80-saline. As a positive control for the *Pig-A* gene mutation assay, mice were given a single oral administration of *N*-nitroso-*N*-ethylurea. At 2 and 8 weeks after treatments, we analyzed CD24-negative and -positive red blood cells in peripheral blood and calculated *Pig-A* mutant frequencies. As a result, we detected no significant differences in the mutant frequencies between C_{60} treated and non-treated mice, indicating that C_{60} is negative for genotoxicity *in vivo* in the limited target tissues assessed in this study. For the full assessment, we need comprehensive whole body survey on the genotoxicity of C_{60}.

Key words: carbon nanoparticle, *in vivo* genotoxicity, *Pig-A* gene mutation assay, fullerene

Introduction

Manufactured nanomaterials are important substances in nanotechnology, and the potential human and environmental risks need to be investigated for risk assessment and management.

There are several reports on the toxicities induced by carbon nanoparticles, such as single-wall carbon nanotubes (SWCNTs), multi-wall carbon nanotubes (MWCNTs) and fullerene (C_{60}). Intraperitoneal application of MWCNTs induced mesothelioma in $p53^{+/-}$ mouse (1) and intrascrotal administration of MWCNTs induced mesothelioma in wild-type rats (2). Reports on the *in vivo* genotoxicity of C_{60}, however, are conflicting. It was reported that intratracheal instillation of C_{60} increased both mutation frequency detected by *gpt*-assay and DNA damage detected by comet assay in lung (3). Nevertheless another group showed that treatment with C_{60} by gavage has no genotoxical effect in ICR mice, using *in vivo* micronucleus test in bone marrow cells (4). These discrepancies could have been caused by differences in administration route, test method, or target organ.

Here we examined the *in vivo* genotoxicity of C_{60} using a different test system—the recently established *Pig-A* gene mutation assay (5,6). The *Pig-A* assay, a powerful tool for the evaluation of *in vivo* genotoxicity, is based on flow cytometric enumeration of glycosylphosphatidylinositol (GPI) anchor-deficient erythrocytes and has been shown to be applicable across species from rodent to monkey (5-8). With this method, we need no transgenic animals to test *in vivo* genotoxicity, but need only 1-2 μL peripheral blood (5,6). Additionally, long-term, accumulated *in vivo* genotoxic effects could be evaluated (9).

Materials and Methods

Test chemicals: Fullerene (C_{60}, Nanom purple SUH; purity >99.9%, Frontier Carbon Corporation, Tokyo, Japan) was obtained and prepared as previously described with some modifications (1). Briefly, C_{60} was suspended to physiological saline (Ohtsuka Pharmaceutical Co., Tokyo, Japan) and autoclaved. After addition of Tween 80 (Polysorbate 80 (HX), NOF Corporation, Tokyo, Japan) at a final concentration of 0.1%, solutions were subjected to sonication by ultrasonic homogenizer (VP30s, TAITEC Co. Japan). C_{60} was prepared at a final concentration of 6 mg/mL. *N*-nitroso-*N*-ethylurea (ENU, Sigma) was dissolved in PBS (pH

[5]Correspondence to: Katsuyoshi Horibata, Division of Genetics and Mutagenesis, National Institute of Health Sciences, 1-18-1 Kamiyoga, Setagaya-ku, Tokyo 158-8501, Japan. Tel: +81-3-3700-1141, Fax: +81-3-3700-2348, E-mail: horibata@nihs.go.jp

6.0) at 10 mg/mL as previously described (5).

Animal treatment: Mice were treated as described previously (1). In brief, 6 male wild-type C57BL/6Cr mice (SLC, Shizuoka, Japan) at the age of 9–11 weeks were given single i.p. injection of 3 mg/head suspension (0.5 mL) of C_{60}. Vehicle solution (0.5 mL) was given to 6 mice as negative controls. As a positive control of this study, 5 mice were given single oral administration of ENU (40 mg/kg). Peripheral bloods were withdrawn from tail vein of mice and analyzed by the *Pig-A* gene mutation assay. All mice were housed individually under specific pathogen-free conditions, with a 12 h light-dark cycle at the animal facility of NIHS. All mice were given tap water and gamma-ray irradiated CRF-1 pellets (Oriental Yeast Co., ltd.) *ad libitum*. Animal experiments were humanely conducted under the regulation and permission of the Animal Care and Use Committee of the National Institute of Health Sciences, Tokyo, Japan.

Antibodies: Anti-mouse TER119 antibody for erythroid cells staining (clone TER-119, PE-Cy7-conjugated) and anti-mouse CD24 antibody (clone M1/69, FITC-conjugated) were obtained from BioLegend.

***Pig-A* gene mutation assay in mice:** Mice *Pig-A* gene mutation assay was performed as previously described (5,8), with some modifications. In brief, EDTA/2K was dissolved in distilled water to make a 12% solution, and used as an anticoagulant. Eighteen μL of peripheral blood were mixed with 2 μL of EDTA solution. Two μL of blood/EDTA mixture was suspended in 0.2 mL of PBS, and the cells were labeled with 1 μg of each anti-mouse TER119 and anti-mouse CD24 antibodies. After incubation for 1 h in the dark at room temperature, the cells were washed once by centrifugation ($500 \times g$, 5 min), resuspended in 2 mL of PBS, and examined using a FACS Canto II flow cytometer (BD Biosciences). After gating for single cells, about 1,000,000 TER119-positive cells were analyzed for the presence of CD24 on their surface. The data were statistically compared with the corresponding solvent control using the Student's t-test.

Results

***Pig-A* gene mutation assay with mice peripheral blood:** Recent works provided that the erythrocyte-based *Pig-A* gene mutation assay is applicable across species (5–8). According to these reports, we modified the original *Pig-A* gene mutation assay and performed it with mice peripheral blood. To classify white blood cells (WBCs) and red blood cells (RBCs) in mice peripheral blood, RBCs were stained with anti-TER119 antibody. Anti-CD24 antibody was used to detect GPI-anchored protein as previously reported (8,10). The gating strategy that was used to score GPI anchor deficient RBCs population was shown in Fig. 1. Single cells including RBCs and WBCs were gated by light scatter (Fig. 1A). To exclude WBCs from this population, TER119-positive cells (Fig. 1B) were analyzed further for the presence on the cell surface of either the GPI-anchored CD24 (Fig. 1C and 1D). The gate used for CD24-negative cells was established by blood cell samples prepared without the fluorescent reagents.

***In vivo* genotoxicity tests on fullerene (C_{60}) analyzed by the *Pig-A* gene mutation assay:** At 2 and 8 weeks after the injection of C_{60} (3 mg/head) and ENU, we analyzed CD24-negative and -positive RBCs in peripheral blood. At both 2 and 8 weeks after the injection, higher amounts of CD24 deficient RBCs were observed in the ENU treated mice (Fig. 1D) as compared with the solvent control (not shown) and C_{60} treated mice (Fig. 1C), respectively. Frequencies of CD24-negative RBCs were summarized in Fig. 2. Frequency of CD24-negative RBCs was significantly increased in ENU treated mice (2 weeks after treatment; $30.12 \pm 3.54 \times 10^{-6}$, and 8 weeks after treatment; $36.64 \pm 15.71 \times 10^{-6}$). However, we detected no obvious differences in frequency of CD24-negative RBCs between C_{60} treated and non-treated mice ($0.25 \pm 0.30 \times 10^{-6}$ versus $0.42 \pm 0.19 \times 10^{-6}$ after 2 weeks and $0.82 \pm 0.54 \times 10^{-6}$ versus $1.87 \pm 1.51 \times 10^{-6}$ after 8 weeks).

These results indicated that although the *Pig-A* gene mutation assay with mouse peripheral blood was appropriately performed, C_{60} was negative for genotoxicity *in vivo* in the RBCs assessed in our study.

Discussion

We demonstrated here that C_{60} (3 mg/head) given intraperitoneally to male C57BL/6Cr mice was negative in the *Pig-A* gene mutation assay using peripheral blood, suggesting that C_{60} was not mutagenic to erythroid precursor cells or hematopoietic stem cells.

The *Pig-A* gene mutation assay is based on detections of GPI-anchored protein on the cell surface of RBCs. The *Pig-A* gene is involved in the synthesis of GPI anchors that link various protein markers to the cell surface. It is known that paroxysmal nocturnal hemoglobinuria (PNH) is caused by somatic *PIG-A* mutations in hematopoietic stem cells (HSCs) and Aerolysin-resistant HSCs from a patient with PNH exhibited clonal *PIG-A* mutations (11,12). Additionally, it is considered that the absence of GPI-anchored protein of RBCs is caused by mutations occurred in the *Pig-A* gene of nucleated erythroid precursors and/or of HSCs (6). These observations suggested that expression of GPI-anchored CD24 of RBCs is depending on the *Pig-A* gene mutations happened in erythroid precursors and/or of HSCs in bone marrows. According to this, we considered that our results, shown here using peripheral blood of mice, reflected genotoxicity of C_{60} on bone marrows.

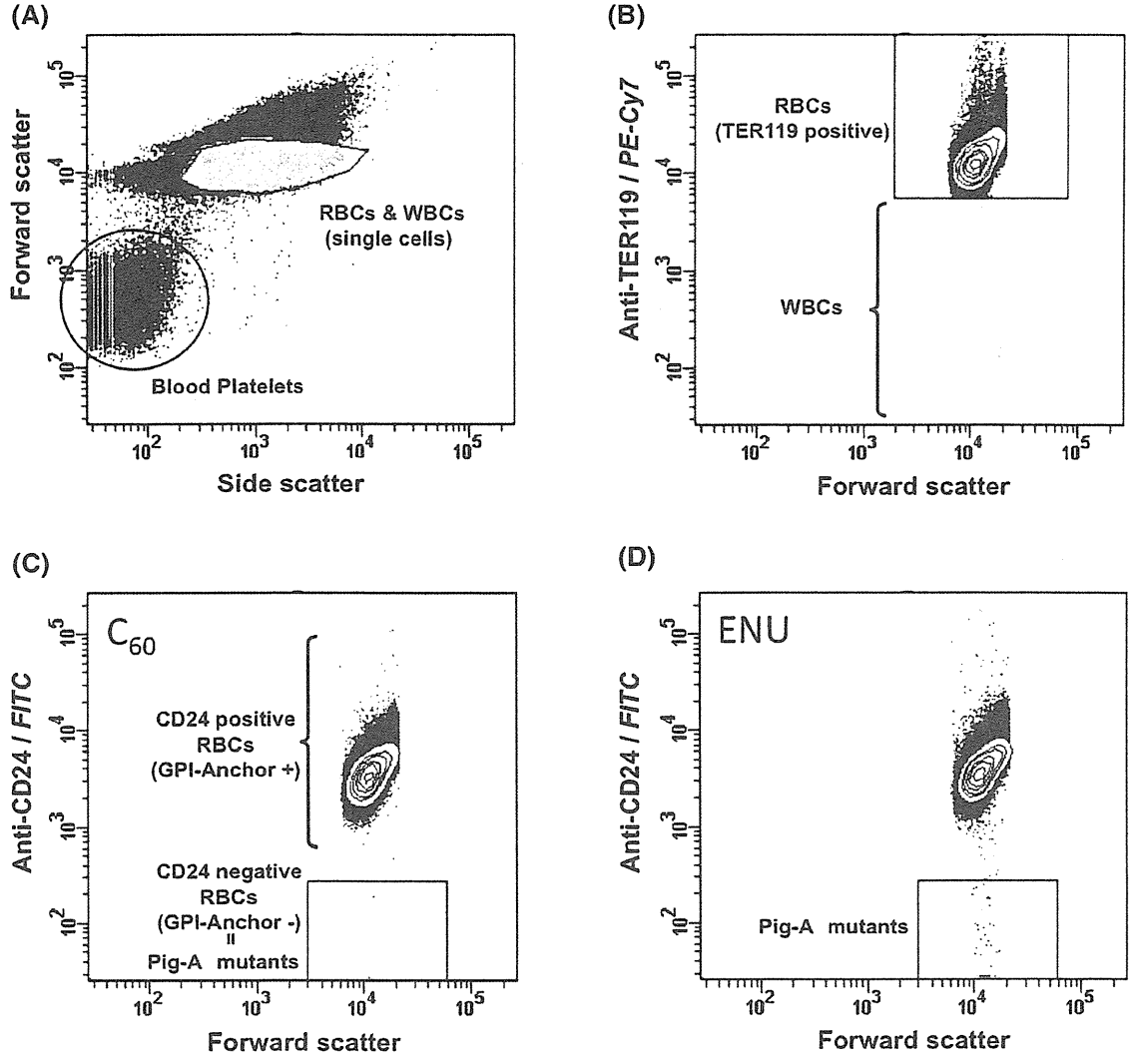

Fig. 1. Analysis of mouse peripheral blood by flow cytometry. (A) Single cell populations were gated and further analyzed with anti-TER119 antibody. (B) TER119-negative white blood cells were excluded from the gated single cell population. TER119-positive red blood cells (RBCs) were gated and further analyzed with anti-CD24 antibody. (C) Approximately 1×10^6 TER119-positive RBCs were analyzed for CD24 expression. CD24-negative RBCs (GPI-Anchor -) were scored as *Pig-A* mutants. In here, there were no obvious features in RBCs derived from C_{60} treated mice. (D) TER119-positive cells derived from ENU-treated mice were analyzed for CD24 expression.

Our data are consistent with the finding that C_{60} administered by gavage to ICR mice is negative in the *in vivo* bone marrow micronucleus test (4). These reports and our result suggest that intraperitoneal injection and gavage of C_{60} are negative for genotoxicity on bone marrow cells including erythroid precursors and HSCs. In both studies, however, the bone marrow was not exposed to C_{60} directly. A recent report showed that intratracheal instillation of C_{60} increased both mutation frequency (*gpt* assay) and DNA damage (comet assay) in the lung (3). From the mutation spectra, it was suggested that oxidative DNA damage might be involved in mutagenicity of C_{60} (3). C_{60}-phagocytized macrophages and granulomatous formations were also observed in the lung (3). Additionally, intratracheal instillation of C_{60} could induce inflammatory responses in the lung (13). It is known that reactive oxygen species (ROS) generation by nanoparticles could be due to particle-cell interactions, especially in the lungs where there is a rich pool of ROS producers like the inflammatory phagocytes, neutrophols and macrophages (14). According to these observations, it is possible that both direct exposure to the target tissue and inflammatory response are important factors in the evaluation of the genotoxicity of C_{60}.

On the other hand, details of inflammatory responses were unclear, but intraperitoneal application of C_{60} induced no obvious change on exposed area except for black patchy deposits on the serosal surfice in $p53^{+/-}$ mouse (1). Therefore it is expected that ROS generation

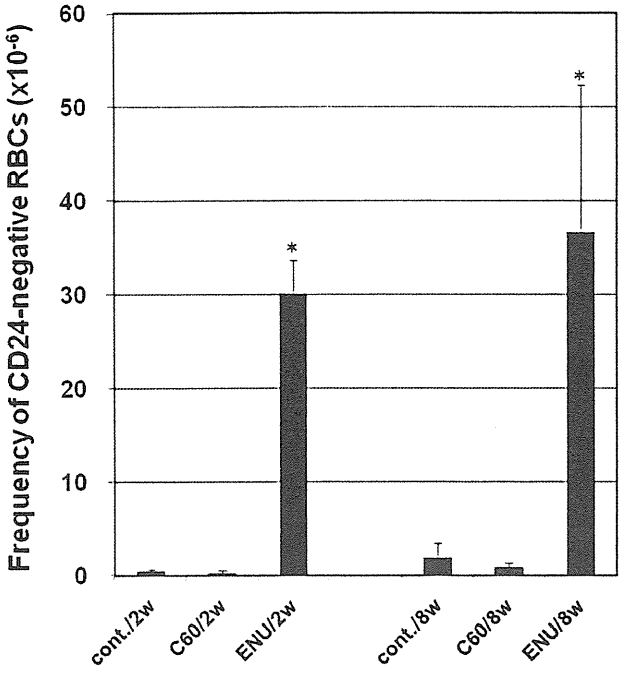

Fig. 2. Frequency of CD24-negative RBCs. At 2 and 8 weeks after mice were treated with C_{60} (3 mg/animal), ENU (40 mg/kg), or solvent, peripheral blood was withdrawn from the tail vein and RBCs were analyzed by flow cytometry for CD24 expression. Values are the mean ± SD of data from 6 animals (C_{60} and solvent) or 5 animals (ENU). *P*-values less than 0.0005 are indicated by asterisks.

by inflammatory responses might not occur and we detected negative genotoxicity in our case.

Recent reports including our results about genotoxicity of C_{60} are discrepant. However, it is known that C_{60} have an ability to quench and generate ROS (15,16). These discrepancies about genotoxicity of C_{60} may be caused by a duality of C_{60} itself. At this time, we cannot explain the mechanism(s) of C_{60} genotoxicity in detail, but we suspect that it is complex and includes oxidative DNA damages, inflammation, and other biological factors. To assess the genotoxicity of C_{60} more fully, we need a comprehensive whole body survey.

Acknowledgement: This work was supported by Health and Labor Sciences Research Grant, Japan, Grant Number: H21-chemical-general-008, and Human Science Foundation, Japan; Grant Number: KHB1006.

References

1 Takagi A, Hirose A, Nishimura T, Fukumori N, Ogata A, Ohashi N, Kitajima S, Kanno J. Induction of mesothelioma in $p53^{+/-}$ mouse by intraperitoneal application of multi-wall carbon nanotube. J Toxicol Sci. 2008; 33: 105-16.

2 Sakamoto Y, Nakae D, Fukumori N, Tayama K, Maekawa A, Imai K, Hirose A, Nishimura T, Ohashi N, Ogata A. Induction of mesothelioma by a single intrascrotal administration of multi-wall carbon nanotube in intact male Fischer 344 rats. J Toxicol Sci. 2009; 34: 65-76.

3 Totsuka Y, Higuchi T, Imai T, Nishikawa A, Nohmi T, Kato T, Masuda S, Kinae N, Hiyoshi K, Ogo S, Kawanishi M, Yagi T, Ichinose T, Fukumori N, Watanabe M, Sugimura T, Wakabayashi K. Genotoxicity of nano/microparticles in *in vitro* micronuclei, *in vivo* comet and mutation assay systems. Part Fibre Toxicol. 2009; 6: 23.

4 Shinohara N, Matsumoto K, Endoh S, Maru J, Nakanishi J. *In vitro* and *in vivo* genotoxicity tests on fullerene C_{60} nanoparticles. Toxicol Lett. 2009; 191: 289-96.

5 Miura D, Dobrovolsky VN, Kasahara Y, Katsuura Y, Heflich RH. Development of an *in vivo* gene mutation assay using the endogenous *Pig-A* gene: I. Flow cytometric detection of CD59-negative peripheral red blood cells and CD48-negative spleen T-cells from the rat. Environ Mol Mutagen. 2008; 49: 614-21.

6 Miura D, Dobrovolsky VN, Mittelstaedt RA, Kasahara Y, Katsuura Y, Heflich RH. Development of an *in vivo* gene mutation assay using the endogenous *Pig-A* gene: II. Selection of *Pig-A* mutant rat spleen T-cells with proaerolysin and sequencing *Pig-A* cDNA from the mutants. Environ Mol Mutagen. 2008; 49: 622-30.

7 Dobrovolsky VN, Shaddock JG, Mittelstaedt RA, Manjanatha MG, Miura D, Uchikawa M, Mattison DR, Morris SM. Evaluation of Macaca mulatta as a model for genotoxicity studies. Mutat Res. 2009; 673: 21-8.

8 Phonethepswath S, Bryce SM, Bemis JC, Dertinger SD. Erythrocyte-based *Pig-a* gene mutation assay: demonstration of cross-species potential. Mutat Res. 2008; 657: 122-6.

9 Miura D, Dobrovolsky VN, Kimoto T, Kasahara Y, Heflich RH. Accumulation and persistence of *Pig-A* mutant peripheral red blood cells following treatment of rats with single and split doses of *N*-ethyl-*N*-nitrosourea. Mutat Res. 2009; 677: 86-92.

10 Keller P, Tremml G, Rosti V, Bessler M. X inactivation and somatic cell selection rescue female mice carrying a Piga-null mutation. Proc Natl Acad Sci U S A. 1999; 96: 7479-83.

11 Takeda J, Miyata T, Kawagoe K, Iida Y, Endo Y, Fujita T, Takahashi M, Kitani T, Kinoshita T. Deficiency of the GPI anchor caused by a somatic mutation of the *PIG-A* gene in paroxysmal nocturnal hemoglobinuria. Cell. 1993; 73: 703-11.

12 Hu R, Mukhina GL, Piantadosi S, Barber JP, Jones RJ, Brodsky RA. *PIG-A* mutations in normal hematopoiesis. Blood. 2005; 105: 3848-54.

13 Park EJ, Kim H, Kim Y, Yi J, Choi K, Park K. Carbon fullerenes (C_{60}s) can induce inflammatory responses in the lung of mice. Toxicol Appl Pharmacol. 2010; 244: 226-33.

14 Li JJ, Muralikrishnan S, Ng CT, Yung LY, Bay BH. Nanoparticle-induced pulmonary toxicity. Exp Biol Med (Maywood). 2010; 235: 1025-33.

15 Markovic Z, Trajkovic V. Biomedical potential of the reactive oxygen species generation and quenching by

fullerenes (C_{60}). Biomaterials. 2008; 29: 3561-73.
16 Singh N, Manshian B, Jenkins GJ, Griffiths SM, Williams PM, Maffeis TG, Wright CJ, Doak SH. NanoGenotoxicology: the DNA damaging potential of engineered nanomaterials. Biomaterials. 2009; 30: 3891-914.

Food and Chemical Toxicology 49 (2011) 1298–1302

Contents lists available at ScienceDirect

Food and Chemical Toxicology

journal homepage: www.elsevier.com/locate/foodchemtox

Lack of promoting effect of titanium dioxide particles on ultraviolet B-initiated skin carcinogenesis in rats

Jiegou Xu [a,e], Yoko Sagawa [b], Mitsuru Futakuchi [a], Katsumi Fukamachi [a], David B. Alexander [a,e], Fumio Furukawa [c], Yoshiaki Ikarashi [d], Tadashi Uchino [d], Tetsuji Nishimura [d], Akimichi Morita [b], Masumi Suzui [a], Hiroyuki Tsuda [e,*]

[a] Department of Molecular Toxicology, Nagoya City University Graduate School of Medical Sciences, 1-Kawasumi, Mizuho-cho, Mizuho-ku, Nagoya 467-8601, Japan
[b] Department of Dermatology, Nagoya City University Graduate School of Medical Sciences, 1-Kawasumi, Mizuho-cho, Mizuho-ku, Nagoya 467-8601, Japan
[c] Daiyukai Institute of Medical Science,Inc., 64 Goura, Nishiazai, Azai-cho, Ichinomiya 491-0113, Japan
[d] National Institute of Health Sciences, 1-18-1 Kamiyoga, Setagaya-ku, Tokyo 158-8501, Japan
[e] Laboratory of Nanotoxicology Project, Nagoya City University, 3-1 Tanabedohri, Mizuho-ku, Nagoya 467-8603, Japan

ARTICLE INFO

Article history:
Received 15 October 2010
Accepted 9 March 2011
Available online 15 March 2011

Keywords:
TiO_2
Nano-size
Skin
Mammary gland
Carcinogenesis
UVB

ABSTRACT

Titanium dioxide (TiO_2) is used in sunscreens and cosmetics as an ultraviolet light screen. TiO_2 has carcinogenic activity in the rat lung, but its effect on the skin has not been reported. We examined the promoting/carcinogenic effect of nano-size TiO_2 particles using a two-stage skin model. c-Ha-*ras* proto-oncogene transgenic (H*ras*128) rats, which are sensitive to skin carcinogenesis, and their wild-type siblings were exposed to ultraviolet B radiation on shaved back skin twice weekly for 10 weeks; then the shaved area was painted with a 100 mg/ml TiO_2 suspension twice weekly until sacrifice. All rats were killed at week 52 except for female H*ras*128 rats which were sacrificed at week 16 because of early mammary tumor development. Skin tumors developed in male H*ras*128 rats and mammary tumors developed in both sexes of H*ras*128 rats and in wild-type female rats, but tumor incidence was not different from controls. TiO_2 particles were detected in the upper stratum corneum but not in the underlying skin tissue layers. TiO_2 particles also did not penetrate a human epidermis model *in vitro*. Our data suggest that TiO_2 does not cause skin carcinogenesis, probably due to its inability to penetrate through the epidermis and reach underlying skin structures.

1. Introduction

Titanium dioxide (TiO_2) is a wide spectrum physical sunscreen (Anderson et al., 1997) and is used in sunscreen formulations to protect against UV radiation-related skin lesions (Gelis et al., 2003; Rouabhia et al., 2002; Suzuki, 1987). TiO_2 nanoparticles have been introduced into sunscreen and cosmetics formulations recently to improve their physical properties, e.g., make them more transparent and less viscous, without losing their UV light blocking ability (Newman et al., 2009). Nanoparticles, defined as having at least one dimension of 100 nm or less (ISO, 2008), were postulated to be able to penetrate the stratum corneum and diffuse into underlying skin structures, which gives rise to concerns about potential health risks (Newman et al., 2009; Nohynek et al., 2008). In human skin samples, topically applied tetramethylammonium hydroxide nanoparticles and sodium bis(2-ethylhexyl) sulfosuccinate nanoparticles get into the hair follicles and the stratum corneum and reach the viable epidermis (Baroli et al., 2007). Dermally administrated near-infrared quantum dot nanoparticles can localize, possibly via skin macrophages and Langerhans cells, to regional lymph nodes (Kim et al., 2004). These findings and the report that endothelial cells have the capacity to internalize nanoparticles (Peters et al., 2004) suggests the possibility of potential pro-inflammatory, cytotoxic or other harmful effects.

TiO_2 particles including micro- and nano-sized, are evaluated as a Group 2B carcinogen by WHO/International Agency for Research on Cancer (IARC) (Baan et al., 2006), based on 2-year animal aerosol inhalation studies (Lee et al., 1985; Pott and Roller, 2005). The mechanism of lung carcinogenesis involves MIP1α derived from TiO_2-laden alveolar macrophages (Xu et al., 2010). Therefore, it is possible that TiO_2 particles may be carcinogenic to the skin and subcutaneous tissues if they penetrate into the epidermis and cause inflammatory lesions, including enhanced macrophage

Abbreviations: TiO_2, titanium dioxide; H*ras*128 rat, human c-Ha-*ras* proto-oncogene transgenic rat; UVB, ultraviolet B light.

* Corresponding author. Tel.: +81 52 836 3496; fax: +81 52 836 3497.
E-mail address: htsuda@med.nagoya-cu.ac.jp (H. Tsuda).

0278-6915/$ - see front matter © 2011 Elsevier Ltd. All rights reserved.
doi:10.1016/j.fct.2011.03.011

activity. Consequently, an important issue is whether TiO_2 particles have the ability to penetrate the stratum corneum and reach the epidermis. Pflucker et al. and Mavon et al. reported that when TiO_2 particles, including micro- and nano-sizes, were topically applied repeatedly to human skin samples *in vitro*, only the upper stratum corneum and hair follicles showed any evidence of particle penetration (Mavon et al., 2007; Pflucker et al., 2001). Even in human skin samples after tape stripping, ultrafine TiO_2 did not penetrate beyond the stratum corneum (Gottbrath and Muller-Goymann, 2003). These results suggest that dermal penetration of TiO_2 particles is in fact associated with hair follicle orifice and not due to direct diffusion through the stratum corneum into the epidermis. Contrary to these *in vitro* findings, Wu et al. reported that TiO_2 nanoparticles could penetrate through the stratum corneum and be located in the deep layer of the epidermis after being topically applied to pig ear *in vivo* for 30 days (Wu et al., 2009). This study also reported that TiO_2 nanoparticles reached different tissues and induced diverse pathological lesions in several major organs after 60 days dermal exposure to hairless mice. The difference in skin penetration between *in vitro* and *in vivo* topical application of TiO_2 particles needs further investigation.

Here, we report results of the carcinogenic effect of TiO_2 particles in the skin using a UVB-initiated 2-stage carcinogenesis protocol. For this purpose, human c-Ha-*ras* proto-oncogene transgenic rats (H*ras* 128) were used because they are more sensitive to chemically induced skin carcinogens than wild-type rats (Park et al., 2004). Our data indicate that TiO_2 did not penetrate through the epidermis and reach the underlying skin structures and did not have skin carcinogenic activity.

2. Materials and methods

2.1. Animals

Transgenic rats carrying the human c-Ha-ras proto-oncogene (H*ras*128 rats), known to be sensitive to chemically induced skin carcinogenesis in males and mammary carcinogenesis in females, and their wild-type counterparts were maintained and bred by CLEA Japan Co., Ltd. (Tokyo, Japan). The animals were housed in the Animal Center of Nagoya City University Medical School and maintained on a 12 h light/12 h dark cycle and received Oriental MF basal diet (Oriental Yeast Co., Tokyo, Japan) and water *ad libitum*. The study was conducted according to the Guidelines for the Care and Use of Laboratory Animals of Nagoya City University Medical School and the experimental protocol was approved by the Institutional Animal Care and Use Committee (H17-28).

2.2. Preparation of titanium dioxide suspension

Ultrafine grade TiO_2 particles (CAS No. 13463-67-7, rutile type, without coating, mean primary diameter of 20 nm, Ishihara Sangyo Kaisha, Ltd., Osaka, Japan) were provided by Japan Cosmetic Association, Tokyo, Japan. TiO_2 particles were suspended at 100 mg/ml in Pentalan 408 (pentaerythritol tetraethylhexanoate, CAS 7299-99-2, Nikko Chemicals Co., Tokyo, Japan). The suspensions were sonicated for 30 min just before use, since TiO_2 particles are known to form aggregates. The size distribution of the TiO_2 suspension in Pentalan 408 was analyzed by a Particle Size Distribution Analyzer (Shimadzu Techno-Research, Inc. Kyoto, Japan.

2.3. Promotion study in the skin

A total of 80 H*ras*128 rats and their wild-type siblings, of both sexes and aged 10 weeks old, were randomly allocated to three groups after a 1 week acclimation: Group 1 received ultraviolet B (UVB) radiation (UVB radiation unit, Dermaray 100, Eisai-Toshiba, Tokyo, Japan) 2 times per week for 10 weeks at 800 mJ/cm^2, 7 min, 20 cm distance from the shaved target skin, followed by painting with 0.5 ml of TiO_2 suspended in Pentalan 408 at 100 mg/ml on the shaved area twice a week until sacrifice. Group 2 received UVB radiation and painting with the vehicle Pentalan 408 on the shaved area twice a week until sacrifice, and Group 3 received painting with 0.5 ml of TiO_2 suspension as in Group1 but without prior UVB radiation. The painting was done gently using a bacterial spreader. The hair of the back was cut in a 3 × 3 cm area with an electric clipper and the remaining hairs were thoroughly shaved with a razor just before every UVB irradiation and/or TiO_2 painting. Any grossly visible papilloma lesions were carefully examined every day (Fig. 1). All the animals were sacrificed at week 52 (after 42 weeks painting) except for the female H*ras*128 rats which were terminated at week 16 (after 6 weeks painting) due to early mammary tumor development. The organs, the skin, brain, lung, liver, mammary gland, mesenterial lymph nodes, spleen and kidney, were excised and fixed in 4% paraformaldehyde solution in PBS buffer adjusted to pH 7.3 and processed for light microscopic examination.

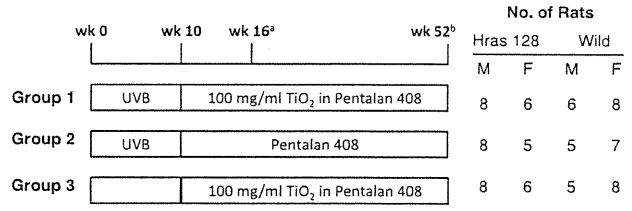

Fig. 1. Schematic of the treatment schedule used to test for skin carcinogenesis in rats. Rats were randomly allocated into three groups: Group 1: UVB radiation for 10 weeks, followed by painting with TiO_2 suspension twice a week; Group 2: UVB radiation for 10 weeks, followed by painting with the vehicle, Pentalan 408, twice a week; and Group 3: painting with TiO_2 suspension twice a week without previous UVB radiation. (a) male H*ras*128 rats and male and female wild-type rats were sacrificed at week 52 and (b) female H*ras*128 rats were sacrificed at week 16 due to early mammary tumor development.

2.4. In vitro TiO_2 penetration assay

To evaluate whether TiO_2 particles could penetrate into the epidermis, the 12 well LabCyte EPI-MODEL (Japan Tissue Engineering Co., Ltd, Aichi, Japan) was used. Eight wells were exposed to either 43.2 μl of Pentalan 408 alone or 100 or 200 mg/ml of TiO_2 suspended in Pentalan 408 for 48 h. The 24 samples in the receiving chambers were then collected for detection of elemental titanium.

2.5. Determination of the elemental titanium

For the detection of elemental titanium, 1 ml of the medium collected from the receiving chambers was treated with 5 ml concentrated HNO_3 for 22 min in a microwave oven. Titanium in the treated solutions was determined by inductively coupled plasma/mass spectrometry (ICP-MS) (HP-4500, Hewlett-Packard Co., Houston, Texas) under the following conditions: RF power-1450 W; RF refraction current-5 W; Plasma gas current-15 L/min; Carrier gas current-0.91 L/min; Peri pump-0.2 rps; Monitoring mass-m/z 48 (Ti); Integrating interval-0.1 s; Sampling period 0.31 s.

2.6. Cytokine analysis

Five wild-type male Sprague–Dawley rats aged 10 weeks were shaved as described above and painted with 0.5 ml of 100 mg/ml of TiO_2 suspended in Pentalan 408 on the shaved area once a day for 14 consecutive days. Five rats were painted with Pentalan 408 as the control. The painted area was excised, rinsed with cold PBS 3 times, and homogenized in 1 ml of T-PER, Tissue Protein Extraction Reagent (Pierce, Rockford, IL, USA), containing 1% (v/v) proteinase Inhibitor Cocktail (Sigma–Aldrich, St Louis, MO, USA). The homogenates were clarified by centrifugation at 10,000g for 5 min at 4 °C. Protein content was measured using a BCA™ Protein Assay Kit (Pierce). The levels of IL-1α, IL-1β, IL-6, GM-CSF, G-CFS, TNFα, IFNγ, IL-18, MCP1, MIP1α, GRO/KC, and VEGF were measured by Multiplex Suspension array (GeneticLab, Co., Ltd., Sapporo, Japan).

2.7. Statistical analysis

Statistical analysis was performed using the Kruskal–Wallis and Bonferroni/Dunn's multiple comparison tests. The statistical significance was analyzed using a two tailed Student's *t*-test and the Bonferroni/Dunn's multiple comparison tests. A P value of <0.05 was considered to be significant.

3. Results

3.1. Size analysis of TiO_2 particles

The size (diameter) of TiO_2 particles suspended in Pentalan 408 ranged from 10 nm to 300 μm, with a mean size of 4.967 ± 0.500 μm and a median size of 4.570 μm, indicating that a large majority of the original nano-size (ultrafine grade) TiO_2 particles formed aggregates in the Pentalan 408 suspension (Fig. 2).

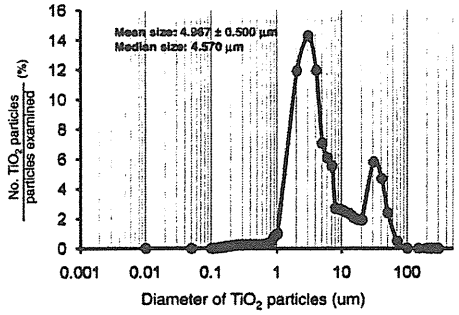

Fig. 2. Size distribution of TiO_2 suspended in Pentalan 408. The size distribution of TiO_2 particles suspended in Pentalan 408 was analyzed by a Particle Size Distribution Analyzer. The mean size was 4.967 ± 0.500 µm and the median size and 4.570 µm.

3.2. Incidence of skin and mammary tumors

In male Hras128 rats, papillomas on the back skin developed from week 32 and the incidence of skin papillomas was 1 out of 8 in Groups 1 and Group 3. No skin tumors were observed on the targeted back skin in female Hras128 rats or wild-type rats of either sex. Eye lid squamous cell papillomas were found in wild-type female rats exposed to UVB (Groups 1 and 2) with incidences of 12.5% and 14.3% (Table 1). No statistically significant inter-group differences in incidence, multiplicity or weight were found (Table 1).

Mammary tumors, diagnosed as adenocarcinomas, were induced with high incidence in Hras128 rats of both sexes. Wild-type female rats also had a relatively high incidence of mammary tumors compared with historical controls of spontaneous mammary tumor development. No statistically significant inter-group differences in incidence, multiplicity or weight were observed (Table 2).

3.3. Tissue analysis of TiO_2 particles

In the rat skin, no inflammatory lesions were observed by histopathological examination. TiO_2 aggregates of various sizes were observed in the upper stratum corneum, but TiO_2 was not found in the underlying epidermis, dermis or subcutaneous tissue (Fig. 3A). Some particles were found in the hair follicles at the level of the granular cell layer in all the TiO_2 treated groups, but not in the deeper parts of the hair follicles or in the surrounding tissue.

In the human epidermis model, TiO_2 aggregates were observed only on the cornified layer of the epidermis, but not in the epidermis (Fig. 3B). The amount of elemental titanium in the receiving chamber did not show any significant difference from the vehicle alone group (Fig. 3C).

Table 2
Mammary tumors in Hras128 and wild-type rats

Sex	Group	Treatment	Incidence[a] (%)	Multiplicity[a] (No./rat)	Weight[a] (g/rat)
Hras128					
Male	1	UVB + TiO_2	4/8 (50)	0.50 ± 0.53	10.50 ± 19.56
	2	UVB	3/8 (36)	0.38 ± 0.51	10.17 ± 17.69
	3	TiO_2	4/8 (50)	0.50 ± 0.53	6.33 ± 14.16
Female	1	UVB + TiO_2	5/6 (83)	1.67 ± 1.37	11.48 ± 20.61
	2	UVB	2/5 (40)	0.60 ± 0.89	0.28 ± 0.53
	3	TiO_2	6/6 (100)	1.33 ± 0.52	4.49 ± 9.76
Wild-type					
Male	1	UVB + TiO_2	0/6	0	0
	2	UVB	0/5	0	0
	3	TiO_2	0/5	0	0
Female	1	UVB + TiO_2	1/8(12.5)	0.13 ± 0.35	0.63 ± 1.80
	2	UVB	1/7(14.3)	0.14 ± 0.38	0.73 ± 1.93
	3	TiO_2	0/8(0)	0	0

[a] Rats died before sacrifice at week 52 were included.

3.4. Cytokine analysis of the rat skin tissue

The levels of 12 inflammatory cytokines (IL-1α, IL-1β, IL-6, GM-CSF, G-CFS, TNFα, IFNγ, IL-18, MCP1, MIP1α, GRO/KC, and VEGF) in the skin of rats receiving TiO_2 treatment is shown in Table 3. TiO_2 treatment did not have a significant effect on the expression of the cytokine levels in the skin compared with the vehicle group.

4. Discussion

TiO_2 particles, nano- and larger scale, are known to be carcinogenic to the rat lung (Baan et al., 2006), and the mechanism of lung carcinogenesis involves MIP1α derived from TiO_2-laden alveolar macrophages (Xu et al., 2010). Thus, they are deemed to have the potential to cause skin tumors after long-term topical application,

Table 1
Skin tumors in Hras128 rats and wild-type rats

Sex	Group	Treatment	Total No. of rats (died before termination)	Survival time (mean week ± SD)	Skin tumor[a]	
					Incidence (%)	Multiplicity (No./rat)
Hras128						
Male	1	UVB + TiO_2	8 (4[b])	47.3 ± 6.8	1/8 (12.5)	0.13 ± 0.35
	2	UVB	8 (4[b])	48.4 ± 5.5	0/8	0
	3	TiO_2	8 (3[b])	48.9 ± 4.7	1/8 (12.5)	0.13 ± 0.35
Female	1	UVB + TiO_2	6	16	0/6	0
	2	UVB	5	16	0/5	0
	3	TiO_2	6	16	0/6	0
Wild-type						
Male	1	UVB + TiO_2	6	52	0/6	0
	2	UVB	5	52	0/5	0
	3	TiO_2	5	52	0/5	0
Female	1	UVB + TiO_2	8 (1[c,d])	51.4 ± 1.8	1/8 (12.5)	0.13 ± 0.35
	2	UVB	7 (1[c],1[d])	51.4 ± 1.5	1/7 (14.3)	0.14 ± 0.38
	3	TiO_2	8	52	0/8	0

[a] Rats died before sacrifice at week 52 were included in statistic calculation of the incidence and multiplicity.
[b] Rats died of mammary tumors between week 33 and week 51.
[c] Rats died of eye lid skin tumors during week 48 and week 50.
[d] Rats died of mammary tumors during week 48.

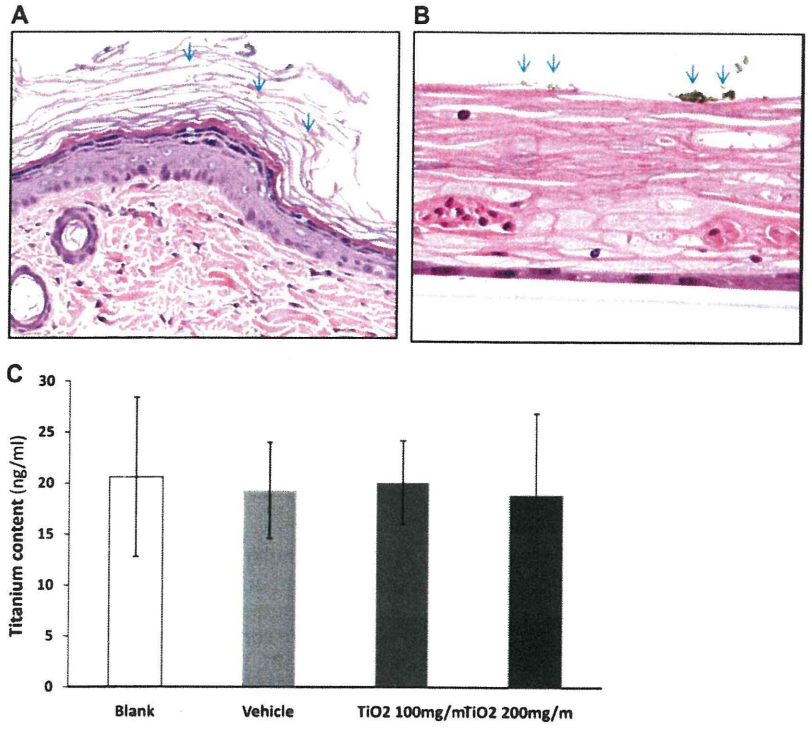

Fig. 3. TiO_2 particles did not penetrate the epidermis. (A) TiO_2 aggregates were observed in the upper stratum corneum, but were not found in the underlying epidermis, dermis or subcutaneous tissue. (B) in the *in vitro* penetration assay, TiO_2 aggregates were localized on the top of the human epidermis model, but not within the epidermis. (C) the amount of elemental titanium detected in the receiving chambers is expressed as mean ± SD. A total of 24 wells of the epidermis model were exposed to the vehicle, 100 mg/ml or 200 mg/ml TiO_2 suspension. Arrows indicate TiO_2 aggregates.

Table 3
Expression level of 12 inflammatory cytokines in the skin treated with Petalan 408 or TiO_2 (5 rats in each group, ng/mg protein)

Cytokine	Pentalan 408	TiO_2 suspension
GM-CSF	23.65 ± 36.48	23.01 ± 16.75
G-CSF	0.37 ± 0.21	0.13 ± 0.16
IL-1α	2914 ± 433	3176 ± 785
IL-1β	38.81 ± 7.49	30.87 ± 7.26
IL-6	1.33 ± 2.97	0.00 ± 0.00
TNFα	29.56 ± 7.75	26.00 ± 8.07
INFγ	5.91 ± 0.68	4.70 ± 1.10
IL-18	845 ± 234	763 ± 299
MCP-1	90 ± 125	123 ± 125
MIP-1α	3.47 ± 7.75	0.00 ± 0.00
GRO/KC	82.66 ± 21.86	63.04 ± 28.76
VEGF	17.96 ± 19.05	14.04 ± 17.55

especially if they induce inflammatory lesions including enhanced macrophage activity in the skin. The present study is the first report of an *in vivo* skin promotion/carcinogenesis study of TiO_2 particles topically applied to the back skin of rats. The incidence of skin tumors in male H*ras*128 was 1 out of 8 (12.5%) in the TiO_2 alone group and in the UVB plus TiO_2 group, higher than that of spontaneously developed skin tumors in these rats (less than 5%) (Park et al., 2004). However, no inter-group difference was observed. Our results demonstrate that TiO_2 suspension does not have a promoting effect on skin carcinogenesis after UVB radiation.

The lack of skin carcinogenesis promotion activity is probably due to lack of penetration of TiO_2 particles through the epidermis to the dermis, where skin tumors arise. Histologically, topically applied TiO_2 particles were located only in the upper stratum corneum and in some hair follicles at the level of granular cell layer, but were not found in the epidermis or the underlying dermis. Our results are consistent with other reports (Mavon et al., 2007; Pflucker et al., 2001). Furthermore, results of the *in vitro* skin model assay used in our study indicate that TiO_2 particles do not penetrate the human epidermis. Since the size of TiO_2 particles was a mixture of nano-size and micro-size, the results indicate that overall the particles do not penetrate through the epidermis and cause an inflammatory response in the skin, although a trace amount of nano-size particles might penetrate the skin tissue. In our study, a large majority of the original nano-size TiO_2 particles (ultrafine grade) formed micro-size aggregates in the Pentalan 408 suspension and this may have affected the particle penetration. The difference between the report of Wu et al. (2009) and ours *in vivo* observation may be ascribed to different test animals, different TiO_2 particles used or different methods of making the TiO_2 particle suspension.

The high incidence of mammary tumors H*ras*128 rats regardless of treatment is attributed to spontaneous development, which is specific to the H*ras*128 rat (Asamoto et al., 2000; Matsuoka et al., 2007; Tsuda et al., 2005).

TiO_2 particle-induced lung carcinogenesis in rats is due to chronic inflammation (ILSI, 2000) with the cytokine MIP1α, derived from TiO_2-laden alveolar macrophages, being an important mediator of carcinogenesis (Xu et al., 2010). In the present study, analysis of 12 inflammatory cytokines, IL-1α, IL-1β, IL-6, GM-CSF, G-CFS, TNFα, IFNγ, IL-18, MCP1, MIP1α, GRO/KC, and VEGF, indicated that no significant change in the expression level of these cytokines occurred after topical application of TiO_2. This result, together with histological observation, indicates that no inflammatory reaction is evoked by topical application of TiO_2. This may partly explain why topical application of TiO_2 suspension has no carcinogenic effect in the skin.

Since tumor promotion activity is considered to be a weak carcinogenic activity (IARC, 1980; Ito et al., 1988, 2003; Konishi et al.,

1987; Nishikawa et al., 1994; Peraino et al., 1971; Pitot et al., 1978; Yamanaka et al., 1996), lack of promotion activity can be interpreted as lack of carcinogenic activity. Thus, the results of our present study indicate that topical application of TiO_2 suspension does not have carcinogenic activity on UVB-treated skin in rats, probably due to lack of penetration through the epidermis. In conclusion, our results indicate that topical application of TiO_2 can be considered to be safe and not carcinogenic to the skin or other organs.

5. Conflict of Interest

The authors declare that there are no conflicts of interest.

Acknowledgement

This work was supported by Health and Labour Sciences Research Grants (Research on Risk of Chemical Substance, H19-kagaku-ippan-006 and H22-kagaku-ippan-005), and Grant-in aid for cancer research from the Ministry of Health, Labour and Welfare, Japan, a grant-in-aid for the Second Term Comprehensive 10-year Strategy for Cancer Control from the Ministry of Health, Labour and Welfare, Japan, and grants-in aid for Cancer Research from the Ministry of Education, Culture, Sports, Science and Technology. Jiegou Xu was a recipient of Bantane Houtokukai Fellowship when this study was performed.

References

Anderson, M., Hewitt, J., Spruce, J., 1997. Broad-spectrum physical sunscreen: titanium dioxide and zinc oxide. In: Lowe, N.J., Shaath, N.A., MA, P. (Eds.), Sunscreens: Development. Evaluation and Regulatory Aspects, New York, Dekker, pp. 357–397.

Asamoto, M., Ochiya, T., Toriyama-Baba, H., Ota, T., Sekiya, T., Terada, M., Tsuda, H., 2000. Transgenic rats carrying human c-Ha-ras proto-oncogenes are highly susceptible to *N*-methyl-*N*-nitrosourea mammary carcinogenesis. Carcinogenesis 21, 243–249.

Baan, R., Straif, K., Grosse, Y., Secretan, B., El Ghissassi, F., Cogliano, V., 2006. Carcinogenicity of carbon black, titanium dioxide, and talc. Lancet Oncol. 7, 295–296.

Baroli, B., Ennas, M.G., Loffredo, F., Isola, M., Pinna, R., Lopez-Quintela, M.A., 2007. Penetration of metallic nanoparticles in human full-thickness skin. J. Invest. Dermatol. 127, 1701–1712.

Gelis, C., Girard, S., Mavon, A., Delverdier, M., Paillous, N., Vicendo, P., 2003. Assessment of the skin photoprotective capacities of an organo-mineral broad-spectrum sunblock on two ex vivo skin models. Photodermatol. Photoimmunol. Photomed. 19, 242–253.

Gottbrath, S., Muller-Goymann, C.C., 2003. Penetration and visualization of titanium dioxide microparticles in human stratum corneum-effect of different formulations on the penetration of titanium dioxide. SOFW J. 129, 11–17.

IARC (1980). Long-term and short-term screening assays for carcinogens: a critical appraisal, 1980/01/01 edn).

ILSI, 2000. The relevance of the rat lung response to particle overload for human risk assessment: a workshop consensus report. ILSI Risk Science Institute Workshop Participants. Inhal. Toxicol. 12, 1–17.

ISO (2008). Nanotechnologies-Terminology and definition for nano-objects-nanoparticle, nanofibre and nanoplate. ISO/TS 27687.

Ito, N., Imaida, K., Tsuda, H., Shibata, M., Aoki, T., de Camargo, J.L., Fukushima, S., 1988. Wide-spectrum initiation models: possible applications to medium-term multiple organ bioassays for carcinogenesis modifiers. Jpn. J. Cancer Res. 79, 413–417.

Ito, N., Tamano, S., Shirai, T., 2003. A medium-term rat liver bioassay for rapid in vivo detection of carcinogenic potential of chemicals. Cancer Sci. 94, 3–8.

Kim, S., Lim, Y.T., Soltesz, E.G., De Grand, A.M., Lee, J., Nakayama, A., Parker, J.A., Mihaljevic, T., Laurence, R.G., Dor, D.M., Cohn, L.H., Bawendi, M.G., Frangioni, J.V., 2004. Near-infrared fluorescent type II quantum dots for sentinel lymph node mapping. Nat. Biotechnol. 22, 93–97.

Konishi, Y., Yokose, Y., Mori, Y., Yamazaki, H., Yamamoto, K., Nakajima, A., Denda, A., 1987. Lung carcinogenesis by *N*-nitroso bis(2-hydroxypropyl)amine-related compounds and their formation in rats. IARC Sci. Publ. 1, 250–252.

Lee, K.P., Trochimowicz, H.J., Reinhardt, C.F., 1985. Pulmonary response of rats exposed to titanium dioxide (TiO_2) by inhalation for two years. Toxicol. Appl. Pharmacol. 79, 179–192.

Matsuoka, Y., Kawaguchi, H., Yoshida, H., Tsuda, H., Tsubura, A., 2007. Rat mammary preneoplasia and neoplasia: a model for human breast cancer research. Trends Cancer Res. 3, 1–13.

Mavon, A., Miquel, C., Lejeune, O., Payre, B., Moretto, P., 2007. In vitro percutaneous absorption and in vivo stratum corneum distribution of an organic and a mineral sunscreen. Skin Pharmacol. Physiol. 20, 10–20.

Newman, M.D., Stotland, M., Ellis, J.I., 2009. The safety of nanosized particles in titanium dioxide- and zinc oxide-based sunscreens. J. Am. Acad. Dermatol. 61, 685–692.

Nishikawa, A., Furukawa, F., Imazawa, T., Yoshimura, H., Ikezaki, S., Hayashi, Y., Takahashi, M., 1994. Effects of cigarette smoke on *N*-nitrosobis(2-oxopropyl)amine-induced pancreatic and respiratory tumorigenesis in hamsters. Jpn. J. Cancer Res. 85, 1000–1004.

Nohynek, G.J., Dufour, E.K., Roberts, M.S., 2008. Nanotechnology, cosmetics and the skin: is there a health risk? Skin Pharmacol. Physiol. 21, 136–149.

Park, C.B., Fukamachi, K., Takasuka, N., Han, B.S., Kim, C.K., Hamaguchi, T., Fujita, K., Ueda, S., Tsuda, H., 2004. Rapid induction of skin and mammary tumors in human c-Ha-ras proto-oncogene transgenic rats by treatment with 7, 12-dimethylbenz[a]anthracene followed by 12-O-tetradecanoylphorbol 13-acetate. Cancer Sci. 95, 205–210.

Peraino, C., Fry, R.J., Staffeldt, E., 1971. Reduction and enhancement by phenobarbital of hepatocarcinogenesis induced in the rat by 2-acetylaminofluorene. Cancer Res. 31, 1506–1512.

Peters, K., Unger, R.E., Kirkpatrick, C.J., Gatti, A.M., Monari, E., 2004. Effects of nano-scaled particles on endothelial cell function in vitro: studies on viability, proliferation and inflammation. J. Mater. Sci.: Mater. Med. 15, 321–325.

Pflucker, F., Wendel, V., Hohenberg, H., Gartner, E., Will, T., Pfeiffer, S., Wepf, R., Gers-Barlag, H., 2001. The human stratum corneum layer: an effective barrier against dermal uptake of different forms of topically applied micronised titanium dioxide. Skin Pharmacol. Appl. Skin Physiol. 14 (Suppl. 1), 92–97.

Pitot, H.C., Barsness, L., Goldsworthy, T., Kitagawa, T., 1978. Biochemical characterisation of stages of hepatocarcinogenesis after a single dose of diethylnitrosamine. Nature 271, 456–458.

Pott, F., Roller, M., 2005. Carcinogenicity study with nineteen granular dusts in rats. Eur. J. Oncol. 10, 249–281.

Rouabhia, M., Mitchell, D.L., Rhainds, M., Claveau, J., Drouin, R., 2002. A physical sunscreen protects engineered human skin against artificial solar ultraviolet radiation-induced tissue and DNA damage. Photochem. Photobiol. Sci. 1, 471–477.

Suzuki, M., 1987. Protective effect of fine-particle titanium dioxide on UVB-induced DNA damage in hairless mouse skin. Photodermatology 4, 209–211.

Tsuda, H., Fukamachi, K., Ohshima, Y., Ueda, S., Matsuoka, Y., Hamaguchi, T., Ohnishi, T., Takasuka, N., Naito, A., 2005. High susceptibility of human c-Ha-ras proto-oncogene transgenic rats to carcinogenesis: a cancer-prone animal model. Cancer Sci. 96, 309–316.

Wu, J., Liu, W., Xue, C., Zhou, S., Lan, F., Bi, L., Xu, H., Yang, X., Zeng, F.D., 2009. Toxicity and penetration of TiO_2 nanoparticles in hairless mice and porcine skin after subchronic dermal exposure. Toxicol. Lett. 191, 1–8.

Xu, J., Futakuchi, M., Iigo, M., Fukamachi, K., Alexander, D.B., Shimizu, H., Sakai, Y., Tamano, S., Furukawa, F., Uchino, T., Tokunaga, H., Nishimura, T., Hirose, A., Kanno, J., Tsuda, H., 2010. Involvement of macrophage inflammatory protein 1alpha (MIP1alpha) in promotion of rat lung and mammary carcinogenic activity of nanoscale titanium dioxide particles administered by intrapulmonary spraying. Carcinogenesis 31, 927–935.

Yamanaka, K., Ohtsubo, K., Hasegawa, A., Hayashi, H., Ohji, H., Kanisawa, M., Okada, S., 1996. Exposure to dimethylarsinic acid, a main metabolite of inorganic arsenics, strongly promotes tumorigenesis initiated by 4-nitroquinoline 1-oxide in the lungs of mice. Carcinogenesis 17, 767–770.

Environmental and Molecular Mutagenesis 52:774–783 (2011)

Research Article

Further Development of the Rat *Pig-a* Mutation Assay: Measuring Rat *Pig-a* Mutant Bone Marrow Erythroids and a High Throughput Assay for Mutant Peripheral Blood Reticulocytes

Takafumi Kimoto,[1]* Satsuki Chikura,[1] Kumiko Suzuki,[1] Xiao mei Kobayashi,[1] Yasuhiro Itano,[1] Katsuyoshi Horibata,[2] Masamitsu Honma,[2] Vasily N. Dobrovolsky,[3] Robert H. Heflich,[3] Daishiro Miura,[1] and Yoshinori Kasahara[1]

[1]*Teijin Pharma Ltd, Tokyo, Japan*
[2]*National Institute of Health Science Japan, Tokyo, Japan*
[3]*National Center for Toxicological Research, U.S. Food and Drug Administration, Jefferson, Arkansas*

Recent studies indicate that the *Pig-a* assay is a promising tool for evaluating in vivo mutagenicity. We have developed novel rat *Pig-a* assays that facilitate measuring mutant frequencies in two early arising populations of blood cells, bone marrow erythroids (BMEs) and peripheral blood (PB) reticulocytes (RETs). In these assays, bone marrow cells of erythroid origin and PB red blood cells (RBCs) were identified using an antibody against rat erythroid-specific marker HIS49. In addition, RETs were selectivity enriched from PB using magnetic separation of cells positive for CD71, a transferrin receptor expressed on the surface of BMEs and RETs, but not on the surface of mature RBCs. With magnetic enrichment, more than 1×10^6 CD71-positive RETs could be evaluated by flow cytometry for *Pig-a* mutant frequency within 5 to 8 min. CD59-deficient RET and BME frequencies of more than 100×10^{-6} and 80×10^{-6} were detected 1 week after treating rats with 40 mg/kg *N*-ethyl-*N*-nitrosourea; by comparison, the frequency of CD59-deficient total RBCs in these rats was 13.2×10^{-6}. The frequency of spontaneous *Pig-a* mutant RETs and BMEs was less than 5×10^{-6} and 15×10^{-6}, respectively. Since ~98% of nucleated cells in the BME fraction were erythroblasts, it should be possible to use BMEs to determine the spectrum of CD59-deficient *Pig-a* mutations in cells of erythroid lineage. Conducting concurrent *Pig-a* assays on RETs and BMEs may be useful for evaluating the in vivo mutagenicity of chemicals, especially when prolonged mutant manifestation is not feasible or when the confirmation of mutation induction is necessary. Environ. Mol. Mutagen. 52:774–783, 2011. Published 2011 Wiley Periodicals, Inc.[†]

Key words: *Pig-a; N-ethyl-N-nitrosourea; reticulocytes; bone marrow erythroids; in vivo gene mutation assay; flow cytometry*

INTRODUCTION

An in vivo mutation assay, using the endogeneous, X-linked *Pig-a* gene as a reporter of mutation, has shown promise for evaluating genotoxicity in laboratory animals [Dobrovolsky et al., 2010b]. Several approaches have been developed for measuring *Pig-a* mutant frequency in peripheral blood (PB) cells. One approach is to evaluate the expression of proteins (in rats, usually CD59) anchored by glycosyl phosphatidyl inositol (GPI) to the surface of peripheral red blood cells (RBCs). The target RBCs are defined by flow cytometry (FCM) using a combination of light scatter to distinguish cells from platelets and debris and by labeling the PB with fluorescent antibodies specific for the common white blood cell (WBC) antigen, CD45, to eliminate leukocytes from the analysis [Miura et al., 2008a]. Using this methodology, we determined that the frequency of CD59-negative (*Pig-a* mutant) PB RBCs increases in a near-additive fashion in rats

Grant sponsor: Japan Health Sciences Foundation; Grant Number KHB1006.

Correspondence to: Takafumi Kimoto, Teijin Pharma Limited, 4-3-2 Asahigaoka, Hino, Tokyo 191-8512, Japan. E-mail: t.kimoto@teijin.co.jp

Received 20 May 2011; provisionally accepted 21 July 2011; and in final form 22 July 2011

DOI 10.1002/em.20677

Published online 5 October 2011 in Wiley Online Library (wileyonlinelibrary.com).

treated with four weekly doses of *N*-ethyl-*N*-nitrosourea (ENU) [Miura et al., 2009]. On the basis of these findings, we proposed a model in which *Pig-a* mutation and the subsequent disruption of GPI synthesis occurs in erythroid precursors and/or stem cells in the bone marrow (BM); GPI-deficient and GPI-anchored-protein-deficient (GPI-AP-deficient) RBCs derived from these *Pig-a* mutants then are supplied continuously to the PB, thus accounting for the kinetics and persistence of CD59-deficient *Pig-a* mutant RBCs observed in treated rats.

Nucleic acid staining with Thiazole Orange or SYTO13 is able to distinguish reticulocytes (RETs) from mature RBCs in the *Pig-a* assay. Combined with leukocyte depletion, staining for RETs made it possible to measure increases in genotoxin-induced *Pig-a* mutation at an earlier time point than was possible in the total RBC assay [Bryce et al., 2008; Phonethepswath et al., 2008, 2010]. On the basis of the relatively rapid increase in RET *Pig-a* mutant frequency, Dertinger et al. [2010] concluded that the RET *Pig-a* assay was an appropriate system for incorporating an in vivo gene mutation endpoint into rat 28-day repeat-dose toxicology studies. The erythrocyte (total RBC and/or RET) *Pig-a* assays can be conducted with small volumes of blood, allowing multiple assays on the same animal. Thus, in vivo gene mutation and general toxicity, in principle, can be evaluated in a single study, resulting in a net decrease in the number of experimental animals required to generate this information.

Another approach to measure RBC *Pig-a* mutant frequency uses the anti-rat erythroid maker, HIS49, to identify erythrocytes in PB [Dobrovolsky et al., 2010a]. In theory, the antibody for this marker also could be used as the basis for developing rat *Pig-a* gene mutation assays for RETs and BM erythroids (BMEs).

RETs are a relatively small fraction of the erythrocytes in PB, which limits the number of RETs that can interrogated for *Pig-a* mutation in a reasonable length of time (e.g., the analysis of 3×10^5 RETs by FCM directly from PB may take 15–20 min). This makes reliable quantitation of spontaneous RET *Pig-a* mutant frequencies difficult and limits the sensitivity of the assay for detecting weak mutagens. In the present study, we have used a protocol for magnetically enriching RETs expressing the CD71 surface antigen [Offer et al., 2005], which enabled us to efficiently interrogate 1×10^6 or more RETs for mutation.

The target cells in FCM erythrocyte *Pig-a* assays (either RETs or mature RBCs) do not contain nuclei; this makes it difficult to confirm the mutational basis of the altered GPI-AP-deficient phenotype by sequencing. Using the mouse as an animal model, we recently described FCM methods for quantifying GPI-AP-deficient BMEs (which contain a high proportion of nucleated cells), sorting out the mutant cells, and analyzing the sorted cells for mutations in the *Pig-a* gene [Kimoto et al., 2011]. In this article, we describe the development of a rat version of the BME *Pig-a* assay and we used the assay for studying the kinetics of *Pig-a* mutant erythroid manifestation in the first 2 weeks after exposing rats to ENU. Finally, we evaluated the cell types in the sorted BMEs to determine the suitability of this fraction for DNA sequence analysis.

MATERIALS AND METHODS

Reagents and Antibodies

ENU and K_2-ethylenediaminetetraacetic acid (EDTA) were purchased from Sigma-Aldrich (St. Louis, MO). Ca^{2+}- and Mg^{2+}-free phosphate-buffered saline (PBS, pH 7.2) was purchased from Invitrogen (Carlsbad, CA). Fetal bovine serum (FBS) was purchased from HyClone (Logan, UT). Anti-rat CD59 antibody (clone TH9, FITC-conjugated), anti-rat CD71 antibody (clone OX-26, PE-conjugated), anti-rat CD45 antibody (clone OX-1, PE-conjugated), anti-rat erythroid marker (clone HIS49, biotin-conjugated), anti-rat CD32 (clone D34-485, purified), streptavidin-APC, streptavidin-PE-Cy7, and 7-AAD (Via-Probe™) were obtained from BD Biosciences (Tokyo, Japan). Anti-rat CD71 antibody (clone OX-26, Alexa Fluor® 647-conjugated) was purchased from BioLegend (Tokyo, Japan).

Animals and Dosing

All experimental procedures were conducted in accordance with the Guiding Principles for the Care and Use of Laboratory Animals (Teijin Pharma Ltd., Tokyo, Japan), and the experimental protocol used in this study was approved by the Committee for Animal Experiments of the Teijin Institute for Biomedical Research. CD(SD) male rats were obtained from Charles River Laboratories (Yokohama, Japan); the rats received feed and water ad libitum. After a 12-day acclimation period, 7-week-old rats were administrated a single dose of 40 mg/kg ENU by gavage. ENU was dissolved in warm (37°C) PBS (pH adjusted to 6.0–6.1) at a concentration of 4 mg/mL (ENU concentration adjusted to account for the water and acetic acid stabilizer in the commercial preparation), and sterilized with a 0.2 μm filter. Control rats were administered an appropriate volume of PBS.

Peripheral Blood and Bone Marrow Collection, Processing, and Labeling

One and two weeks after ENU administration, PB was collected from the tail vein of all animals and BM from the femurs of 3/group (control and ENU-treated). The PB collection was conducted as described in our previous report [Kimoto et al., 2011].

A summary and highlights of the PB and BM *Pig-a* assays are shown in Figure 1 and Table I, respectively. The staining of total RBCs was similar to our previous report [Dobrovolsky et al., 2010a]. Three microliters of blood/EDTA mixture were suspended in 200 μL of PBS, and the cells were labeled with 1 μg of FITC-conjugated anti-rat CD59 and 0.25 μg of biotinylated HIS49 antibody. After incubation for 1 hr in the dark at room temperature, the samples were washed with PBS, centrifuged 5 min at 1,680*g*, and resuspended in 200 μL of PBS; 0.25 μg of APC-conjugated streptavidin were added, and the samples were incubated for 15 min in the dark at room temperature. The cell samples then were centrifuged 5 min at 1,680*g* and resuspended in 1 mL of PBS.

For RETs enrichment and labeling, 30 μL of blood/EDTA were mixed with 200 μL of PBS; the cell suspension was layered on Lympholyte-Mammal (Cedarlane Laboratories; Burlington, Ontario, Canada) and centrifuged to separate the nucleated cells and platelets from RBCs according to the manufacturer's instructions. The RBC fraction was washed

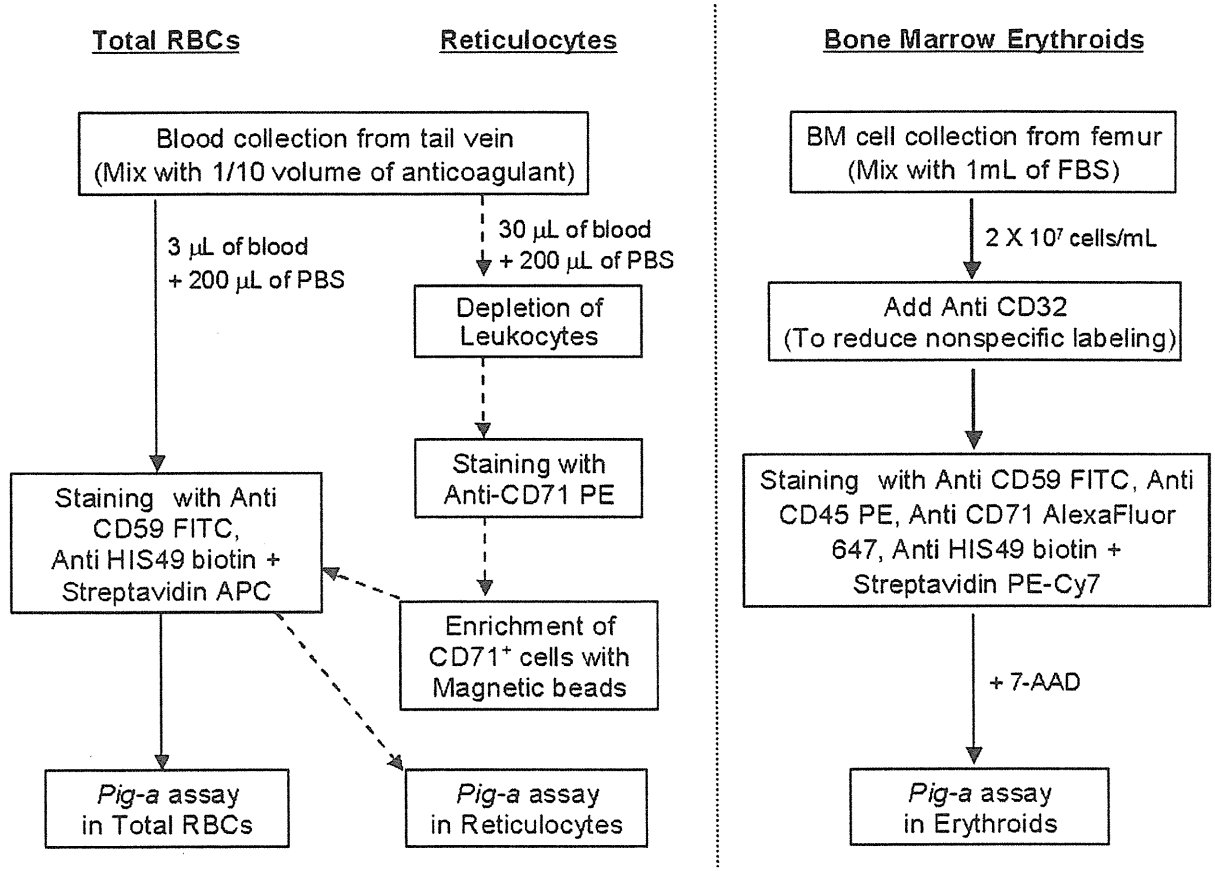

Fig. 1. Sample preparation flow chart for various *Pig-a* assays. Peripheral blood (PB) was used for measuring *Pig-a* mutation in total red blood cells (RBCs) and reticulocytes (RETs). Bone marrow (BM) cells were used for measuring *Pig-a* mutation in bone marrow erythroids (BMEs). Details of the sample preparation are described in Materials and Methods.

TABLE I. Highlights of *Pig-a* Mutant Assays Described in this Communication

Target Population	Fluorescently conjugated antibodies and other reagents	Compensation	Cells interrogated in <10 min
Total red blood cells	FITC anti-CD59 Biotin anti-erythroid marker (HIS49) Streptavidin-APC	No (2 colors)	>1 Million
Reticulocytes	FITC anti-CD59 PE anti-CD71 Biotin anti-erythroid marker (HIS49) Streptavidin-APC	Yes (3 colors)	>1 Million
Bone marrow erythroids	FITC anti-CD59 PE anti-CD45 7-AAD Biotin anti-erythroid marker (HIS49) Streptavidin-PE-Cy7 Alexa Fluor® 647anti-CD71	Yes (5 colors)	300,000

with PBS and 100 μL of suspension were placed in a new tube containing 1 μg of PE-conjugated anti-rat CD71 and incubated for 15 min on ice. Labeled cells were washed with 2 mL of 1 × IMag™ Buffer (BD Biosciences) and centrifuged (1,680*g*, 5 min), the supernatant fluid removed, and the cells were mixed with 50 μL of BD IMag™ PE Particles Plus-DM (BD Biosciences). The suspension was incubated for 15 min in a refrigerator and the fraction of CD71-positive cells was enriched using a BD IMagnet™ magnetic stand (BD Biosciences)

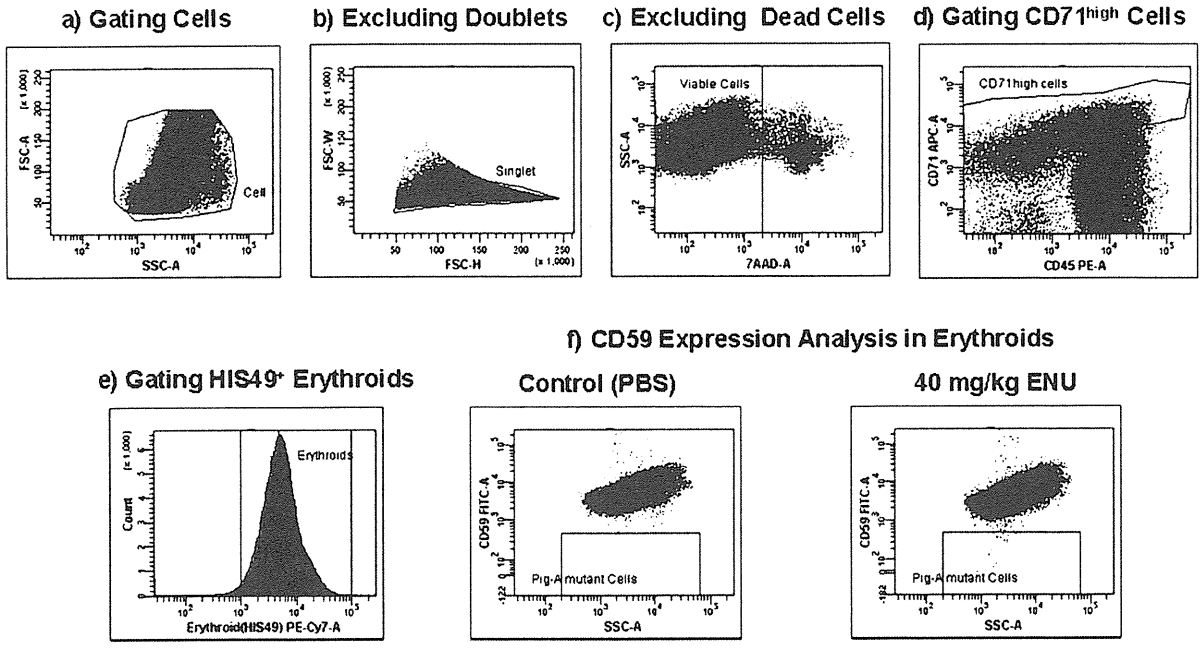

Fig. 2. Typical cytograms for identification of *Pig-a* mutant bone marrow erythroids (BMEs). The cytograms in panels 1 through 6 outline consecutive steps for refining the population of target BMEs and enumerating the mutants (details can be found in the text). Note the low number of CD59-deficient cells (presumed *Pig-a* mutants) in control animals and the increased number of mutants in rats treated with 40 mg/kg ENU-treated (panel **2f**).

according to manufacture's suggested positive selection method. Enriched samples were labeled with HIS49 and anti-CD59 antibodies as indicated for total RBC labeling, with the exceptions that the incubation time for labeling enriched RETs was half that for total RBCs and the final volume of cell suspension was 500 μL.

BMEs were collected from rat femurs by flushing with 1 mL of FBS, followed by washing with 1 mL of PBS containing 2% FBS. The samples were centrifuged once at 420*g* for 5 min, and then diluted to ~2 × 10^7 cells/mL; 100 μL of these samples then were incubated at 4°C for 5 min with 1 μg of anti-rat CD32 to reduce subsequent nonspecific labeling with fluorescent antibodies. The cells were further labeled with 2 μg of PE-conjugated anti-rat CD45, 1 μg of Alexa Fluor® 647-conjugated anti-rat CD71, 2 μg of FITC-conjugated anti-rat CD59, and 0.25 μg biotinylated HIS49 antibodies. After incubation for 30 min at 4°C, the cells were washed, resuspended in PBS/2% FBS containing 1 μg of PE-Cy7-conjugated streptavidin, and incubated for a further 15 min. Washed cell samples were pelleted, resuspended in 500 μL of PBS containing 2% FBS, and then mixed with 40 μL of BD Via-Probe™ for the analysis by FCM.

Flow Cytometry

FCM analysis of CD59-negative total RBCs and RETs was conducted on a FACSCanto™ II flow cytometer equipped with 405 nm violet, 488 nm blue, and 635 nm red lasers. The detection of CD59-negative BMEs was conducted using a FACSAria™ I flow cytometer equipped with 405 nm violet, 488 nm blue, and 635 nm red lasers (both instruments from BD Biosciences). All gates for detecting CD59-negative mutants were set using unstained and single-antibody-stained samples before evaluating the multi-antibody-labeled samples. Analysis of RETs and BMEs was performed after fluorescence compensation adjustment in FACSDiva (ver. 4.0 for FACSAria I, ver. 5.0 for FACSCanto II).

Sorting BMEs and Evaluation of the Frequency of Nucleated Cells

Sorting of the BME population was conducted on a FACSAria I according to the manufacturer's instructions. BM cells were collected from three untreated CD(SD) male rats and stained with antibodies as described above. The sorting precision mode was set as "purity," sheath pressure was set to 20 psi, and a 100 μm nozzle was used. For each sample, up to 1 × 10^5 $CD71^+$/$HIS49^+$ cells (defined as erythroids in Fig. 2e) were sorted into a 1.5 mL tube containing 500 μL of PBS/2% FBS. The sorting procedure was repeated three times for samples derived from each animal. The cells were pelleted by centrifugation (5 min, 420*g*), and then resuspended in 500 μL of PBS/2% FBS. The samples were loaded into 1 mL Fluid Chambers and processed in a Cyto-Tek® centrifuge (Sakura Finetek, Tokyo, Japan) for gentle cell transfer onto glass slides. The slides were stained with May-Grünwald and Giemsa. Microscopic observations were performed to discriminate between nucleated cells and non-nucleated cells.

RESULTS

FCM Analysis of BMEs and RETs for *Pig-a* Mutants

Figures 2 and 3 show the FCM gating strategies for analyzing *Pig-a* mutant BMEs and RETs, respectively. The BME phenotype was defined as positive for both CD71 and HIS49. For analysis of BMEs, cells were first gated by their forward and side light scatter properties (Fig. 2a), then doublets were discriminated on a FSC-H vs. FSC-W cytogram (Fig. 2b). Dead cells were excluded by staining with 7-AAD

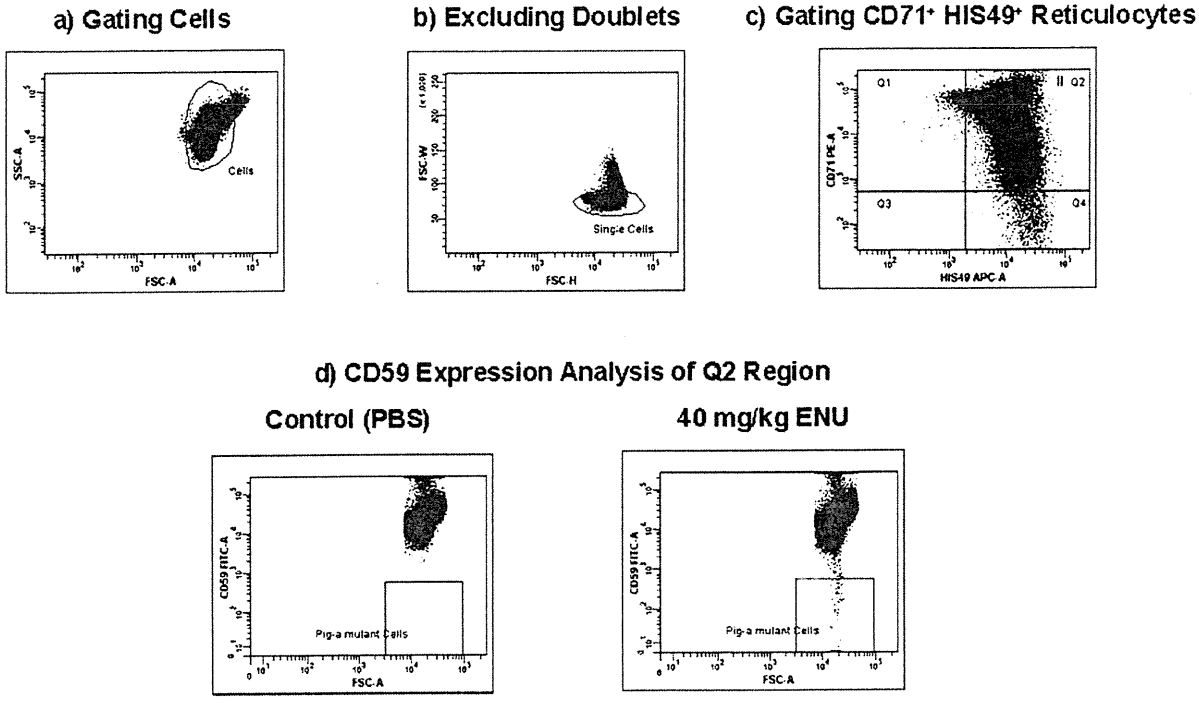

Fig. 3. Typical cytograms for identification of *Pig-a* mutant reticulocytes (RETs). The four cytograms outline consecutive steps for refining the population of target RETs and enumerating the mutants (details can be found in the text). Note the low number of CD59-deficient cells (presumed *Pig-a* mutants) in control animals and the increased number of mutants in rats treated with 40 mg/kg ENU (panel **3d**).

(Via-Probe™; Fig. 2c), and viable cells were analyzed for the expression of CD45 and CD71 (Fig. 2d). $CD71^+$ cells were further analyzed for HIS49 expression to include only the cells of erythroid lineage (Fig. 2e). Finally, $\sim 3 \times 10^5$ $CD71^+/HIS49^+$ BMEs were interrogated for the expression of CD59: the number of CD59-deficient BMEs increased in rats treated with 40 mg/kg ENU (Fig. 2f).

RETs, like BMEs, have a $CD71^+/HIS49^+$ phenotype. For analysis of RETs from CD71-enriched peripheral blood samples, a single-cell population was gated by consecutive light scatter cytograms, FSC-A/SSC-A (Fig. 3a) and FSC-H/FSC-W (Fig. 3b), as was done for the analysis of BMEs. Single cells were further analyzed for CD71 and HIS49 expression to gate $CD71^+/HIS49^+$ RETs, which were located in the Q2 region of the cytogram shown in Figure 3c. Analysis of $CD71^+/HIS49^+$ RETs for the expression of CD59 is shown in Figure 3d. The RET enrichment protocol enables the interrogation of more than 1×10^6 $CD71^+/HIS49^+$ cells in less than 10 min. The number of CD59-negative RETs was increased in samples from rats treated with 40 mg/kg ENU (Fig. 3d).

Frequency of Nucleated Cells among $CD71^+/HIS49^+$ BMEs

The $CD71^+/HIS49^+$ BME population defined by our FCM protocol potentially includes both nucleated cells like erythroblasts and non-nucleated cells like RETs. Therefore, we sorted the $CD71^+/HIS49^+$ BME population using a FACSAria I cell sorter, and then examined the sorted cells microscopically. Figure 4a shows sorted cells stained by the May-Grünwald and Giemsa method. Based on evaluation of a total of 3,000 cells from each of three untreated rats, the percentages of cell types among the sorted $CD71^+/HIS49^+$ BME population were as follows: erythroblasts, 63.5 ± 3.9%; other nucleated cells (irregular nuclear shape consistent with leukocyte profiles), 1.4 ± 0.7%; and RETs, 35.1 ± 4.0% (Fig. 4b). Among nucleated cells, ~98% were erythroblasts.

Frequencies of *Pig-a* Mutant RBCs, RETs, and BMEs in Rats Treated with ENU

Figure 5 and Table II show *Pig-a* mutant frequencies in total RBCs, RETs, and BMEs at 1 and 2 weeks after dosing with 40 mg/kg ENU or PBS vehicle. Also, the spontaneous frequencies of CD59-negative PB RBCs were analyzed before the treatments, and all of the animals had normal *Pig-a* mutant frequencies (i.e., less than 10×10^{-6}; data not shown). The frequencies of CD59-negative RBCs, RETs, and BMEs at 1 week after dosing with ENU were $(13.2 \pm 3.8) \times 10^{-6}$, $(124.8 \pm 20.7) \times 10^{-6}$, and $(84.4 \pm 26.7) \times 10^{-6}$, respectively. At 2 weeks after

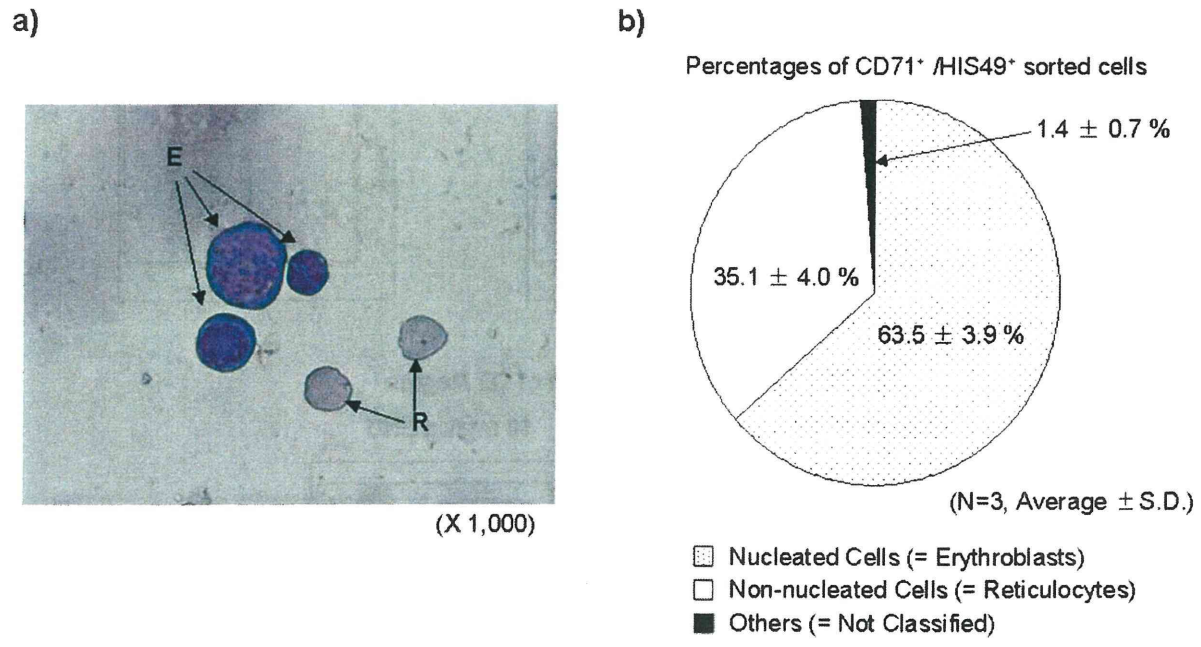

Fig. 4. Microscopic analysis of flow-sorted bone marrow erythroids. (**a**) Bright field visualization of sorted $CD71^+/HIS49^+$ cells that were stained with May-Grünwald and Giemsa. "E" points to erythroblasts with representative nuclear and cytoplasmic characteristics. "R" points to reticulocytes. (**b**) Percentages of cells among sorted $CD71^+/HIS49^+$ cells. Each percentage is the mean ± SD of data from three rats (N = 3). A total of 3,000 cells from each animal were characterized and classified. "Others" contained nucleated cells with irregular nuclear shapes (consistent with leukocyte profiles).

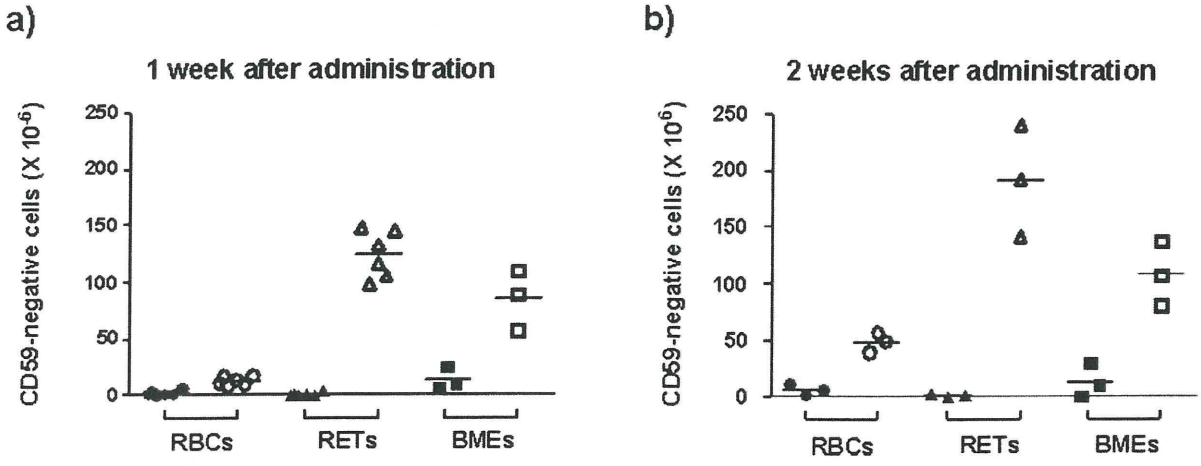

Fig. 5. Frequencies of *Pig-a* mutant red blood cells (RBCs), reticulocytes (RETs), and bone marrow erythroids (BMEs) from control and 40 mg/kg ENU-treated Rats. (**a**) 1 week after administration (N = 6 for RBCs and RETs; N = 3 for BMEs), (**b**) 2 weeks after administration (N = 3). Solid symbols are data from the control group; open symbols are data from the ENU-treated group. The circle, the triangle and square are mutant frequencies for RBCs, RETs, and BMEs, respectively, from individual rats.

ENU dosing, the frequencies of CD59-negative RBCs, RETs, and BMEs were (48.7 ± 9.1) × 10^{-6}, (191.3 ± 49.0) × 10^{-6}, and (107.8 ± 28.3) × 10^{-6}, respectively. The frequency of CD59-negative RBCs increased 3.7-fold between Week 1 and Week 2. During the same period, the frequencies of CD59-negative RETs and BMEs increased only 1.5- and 1.3-fold, respectively.

The background *Pig-a* mutant frequency for RETs was the lowest and least variable of the three cell types. The frequencies of CD59-negative cells in vehicle-treated rats

TABLE II. *Pig-a* Mutant Frequencies in Peripheral Total Red Blood Cells (RBCs), Reticulocytes (RETs), and Bone Marrow Erythroids (BMEs) for Individual Rats Treated with Phosphate Buffered Saline (PBS) Vehicle or 40 mg/kg *N*-Ethyl-*N*-nitrosourea (ENU)

		Pig-a mutant frequency at 1 week after treatment ($\times 10^{-6}$)			*Pig-a* mutant frequency at 2 weeks after treatment ($\times 10^{-6}$)		
Group	Animal no.	RBCs	RETs	BMEs	RBCs	RETs	BMEs
PBS	01	4	2	6.7	—	—	—
	02	1	4	10.0	—	—	—
	03	2	1	24.9	—	—	—
	04	2	0	—	7	2	30.0
	05	7	0	—	12	3	10.0
	06	2	0	—	2	0	0.0
	Ave.	3.0	1.2	13.9	7.0	1.7	13.3
	S.D.	2.2	1.7	9.7	5.0	1.5	15.3
	S.E.	0.8	0.6	4.6	2.4	0.7	7.2
ENU (40 mg/kg)	11	14	146	56.7	—	—	—
	12	18	106	86.7	—	—	—
	13	10	133	110.0	—	—	—
	14	17	148	—	57	240	136.7
	15	9	117	—	39	192	80.0
	16	11	99	—	50	142	106.7
	Ave.	13.2	124.8	84.4	48.7	191.3	107.8
	S.D.	3.8	20.7	26.7	9.1	49.0	28.3
	S.E.	1.4	7.7	12.6	4.3	23.1	13.4

—, no data; S.D., standard deviation; S.E., standard error.

at 1 and 2 weeks after dosing for RBCs were (3.0 ± 2.2) × 10^{-6} and (7.0 ± 5.0) × 10^{-6}; for RETs, (1.2 ± 1.7) × 10^{-6} and (1.7 ± 1.5)×10^{-6}; and for BMEs, (13.9 ± 9.7) × 10^{-6} and (13.3 ± 15.3) × 10^{-6}.

Correlation Between *Pig-a* Mutant Frequency of RETs and BMEs

Based on the individual data points shown in Table II, a correlation between pairs of *Pig-a* mutant RETs vs. BMEs was evaluated (Fig. 6). A significant correlation was observed between these two sets of data (r^2 = 0.8316).

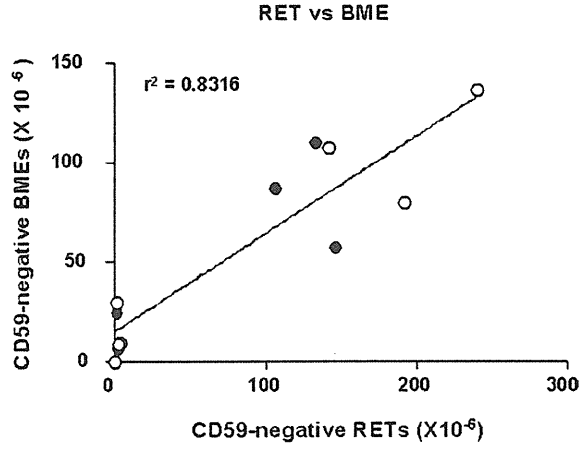

Fig. 6. Correlation between the frequencies of *Pig-a* mutant reticulocytes and bone marrow erythroids at 1 and 2 weeks after treatment with a single dose of *N*-ethyl-*N*-nitorosourea. Data were derived from individual rats shown in Table II. Correlation coefficients (r^2) are indicated on the graph. Solid symbols are data from Week 1; open symbols are data from Week 2.

DISCUSSION

In this study, we developed new *Pig-a* assays for rat RETs and BMEs; both assays use a combination of antibodies to CD71 and the erythroid marker HIS49. Consistent with our model for the generation of erythrocyte *Pig-a* mutations [Miura et al., 2009], we confirmed that increased *Pig-a* mutant frequencies in ENU-treated rats are detected in RETs and BMEs earlier than in total RBCs. Furthermore, microscopic examination of the sorted $CD71^+/HIS49^+$ BME population revealed that over 60% of cells were nucleated cells and ~98% of nucleated cells were erythroblasts. These observations indicate that the $CD71^+/HIS49^+$ fraction of BMEs is amenable for the molecular analysis of *Pig-a* gene mutation in the erythroid lineage.

We previously reported on the increased frequencies of CD59-negative RBCs in rats after ENU administration [Miura et al., 2008a, 2009]. Although this study also measured *Pig-a* mutant frequency in ENU-treated rats, direct comparisons between the mutant frequencies detected in the studies are complicated by differences in experimental design, e.g., ENU dose and exposure route,

strain of rat. In another previous report, we described a *Pig-a* assay for mouse BMEs in which *Pig-a* mutants are identified by the deficiency of another GPI-AP marker, CD24 [Kimoto et al., 2011]. The mouse assay also uses a combination of antibodies to an erythroid marker, TER-119 [Kina et al., 2000], and the transferrin receptor, CD71. This approach was shown to be a reliable method for identifying BMEs in mice. In the mouse study, we determined sequence changes in *Pig-a* cDNA from flow-sorted CD24-negative BMEs derived from ENU-treated animals. In other work, we described methods for *Pig-a* cDNA sequence analysis in rat splenocytes [Miura et al., 2008b, 2011]. Thus, methods are in place to perform sequence analysis (and determine the spectrum of mutation) of the *Pig-a* gene in rat BMEs. The analysis may prove useful for establishing the mutational origin of the CD59-deficient phenotype measured in the rat RBC and RET *Pig-a* assays.

A rat *Pig-a* assay for RETs was first described by Bryce et al. [2008]. They used Thiazole Orange, which specifically stains nucleic acids, to discriminate between RETs and mature RBCs. In contrast, the method we describe here, which is hereafter referred to as "PIGRET," uses anti-CD71 to identify and enrich RETs from PB. The microscopic evaluation of flow-sorted BMEs suggests that the combination of antibodies to HIS49 and CD71 is a useful tool for recognizing the phenotype of early erythroid cells (Fig. 4). In the PIGRET assay, however, PB is enriched for cells expressing CD71 before labeling with other antibodies for determining the frequency of CD59-deficient CD71-positive RETs. The magnetic enrichment step enables the PIGRET assay to interrogate more than 1×10^6 RETs per sample for CD59 expression in 5–8 min, a 5–10-fold increase in throughput compared with the RET assay described by Phonethepswath et al. [2010]. The frequencies of CD59-negative RETs determined in the PIGRET assay were similar to those reported for RETs by Bryce et al. [2008] and Phonethepswath et al. [2010] using Thiazole Orange and SYTO13, respectively, to identify RETs. The SYTO 13 RET *Pig-a* assay is presently being used in an international collaborative study to evaluate the reproducibility and transferability of the assay [Dertinger and Heflich, 2011]. The interrogation of a larger number of RETs in the PIGRET assay should result in a higher statistical power and, potentially, should detect weak mutagens more reliably than the original SYTO 13 RET *Pig-a* assay.

Dertinger et al. [2011] recently reported a different approach to improve the throughput of the RET *Pig-a* assay. Instead of concentrating the target cell population (i.e., RETs), they used a wild-type cell depletion strategy to enrich the sample for mutant cells. To estimate a mutant frequency, counting beads are added to the sample before the enrichment and used to estimate the wild-type RBC and RET 'cell equivalents' interrogated by the assay. Their method is capable of interrogating the equivalent of over 3×10^6 RETs and 100×10^6 RBCs in a single PB sample. It presently is unclear if one enrichment approach has a clear advantage over the other for using rat RETs to evaluate in vivo mutagenicity. Both assays involve extra materials and processing steps; the PIGRET assay directly measures RET *Pig-a* mutant frequencies while the Dertinger method evaluates a greater number of RETs (as well as total RBCs), but does so indirectly, using a mathematical correction factor.

The new assays detected apparent increases in RET and BME *Pig-a* mutant frequency to $\sim 100 \times 10^{-6}$ one week after treatment with ENU (Fig. 5 and Table II). At this sampling time, the frequency of CD59-negative RBCs was still quite low (13.2×10^{-6}). In the model describing mutation induction in the rat *Pig-a* assay [Miura et al., 2009; Phonethepswath et al., 2010], *Pig-a* mutations are fixed in erythroid precursor cells and mutants proliferate and differentiate in BM. Mutants then transit from the BM into the periphery mainly as RETs, and slowly accumulate in PB, resulting first in an increase in the RET *Pig-a* mutant frequency and later in the total RBC *Pig-a* mutant frequency. The results of the present study support the model because, even 1 week after dosing, the frequencies of *Pig-a* mutant RETs and BMEs were already high (and higher than that of total RBCs), and the only substantial increase in the frequency of *Pig-a* mutant cells between Week 1 and Week 2 was for the total RBCs. From a practical standpoint, these findings demonstrate that RET and BME *Pig-a* mutant frequencies are useful for evaluating the mutagenic potential of test agents at an earlier time than for total RBCs, with the BME assay being, potentially, the earliest in detecting an effect.

At present, it is unclear how early BME mutant frequencies can be sampled with reasonable sensitivity; it may be within day(s) after treatment, e.g., in transgenic mouse reporter assays, the maximum response in BM is detected 3 days after treatment [Thybaud et al., 2003]. If the same is true for *Pig-a* mutant manifestation in BMEs, then it might be possible to integrate the BME *Pig-a* assay into acute-dose in vivo micronucleus assays, as is being proposed for the in vivo Comet assay [Rothfuss et al., 2011], and measure an additional, complementary endpoint, gene mutation. Another uncertainty about the BME *Pig-a* assay is its relatively high spontaneous mutant frequency and high animal-to-animal variability. We are currently working on enhancements to the method with the hope of addressing these issues.

A puzzling observation from our study was that ENU treatment of rats produced somewhat higher RET *Pig-a* mutant frequencies than BME *Pig-a* mutant frequencies. It is not clear why this was the case; however, we can think of at least two potential explanations for these

observations, and these explanations are not mutually exclusive. First, disproportional growth and differentiation of single *Pig-a* mutant BME clones may result in a relative increase in the fraction of *Pig-a* mutant RETs compared with the fraction of mutant BMEs, especially when the BME mutant fraction is measured some time after differentiation and expansion of damaged BMEs has occurred (as was probably the case in our study). A report by Keller et al. [2001] supports the possibility that clonal expansion of *Pig-a* mutant cells at different hematopoietic stages can influence *Pig-a* mutant frequencies determined in various blood cells. In addition, data from our mouse BME experiment indicate that, in ENU-treated animals, multiple CD24-negative cells may have the same *Pig-a* mutation, presumably due to clonal expansion of a single mutation [Kimoto et al., 2011]. Another possibility is that committed BME progenitors, rather than BME stem cells are more highly mutagenized by single doses of ENU. At one week after the treatment, the more highly mutagenized BMEs would have transited to the periphery and be more likely to be detected as RETs than as BMEs. A more detailed monitoring of *Pig-a* mutant frequency manifestation or mutational spectra studies in these cells to monitor the frequencies of clonal expansion may provide additional insight to support one or both of these hypotheses.

In this study, the PIGRET assay enabled us to interrogate more than 1×10^6 RETs for *Pig-a* mutation in 5–8 min. The sensitivity of the PIGRET assay appeared to be better than the BME assay because of a lower spontaneous background mutant frequency. This lower spontaneous frequency may be influenced by the greater number of cells assayed in the PIGRET assay. Our PIGRET spontaneous mutant frequencies were well under 5×10^{-6} and displayed less variability than BME frequencies from individual rats (Table II). In addition, given the high correlation between RET and BME mutant frequencies (Fig. 6), we anticipate that the PIGRET assay may serve as a tool for detecting mutagenic changes in BM.

In summary, we have developed assays for measuring *Pig-a* mutation in rat RETs and BMEs, and showed that these assays can detect ENU-induced increases in *Pig-a* mutant frequency at an earlier stage than the *Pig-a* assay with total RBCs. In particular, methods like PIGRET that measure mutation in earlier-responding cell populations may be useful for integrating the *Pig-a* assay into standard in vivo toxicology assays, where the analysis of mature RBC mutants may not be feasible. Although remarkable progress has been made in the last few years, further refinement of labeling, enrichment, gating methodologies and statistical approaches is needed to make *Pig-a* mutation detection assays suitable for reliable and cost-effective integration into 3-, 14-, or 28-day repeat-dose in vivo studies.

ACKNOWLEDGMENTS

The views presented in this article do not necessarily reflect those of the U.S. Food and Drug Administration.

REFERENCES

Bryce SM, Bemis JC, Dertinger SD. 2008. In vivo mutation assay based on the endogenous *Pig-a* locus. Environ Mol Mutagen 49:256–264.

Dertinger SD, Heflich RH. 2011. In Vivo Assessment of *Pig-a* Gene Mutation - Recent Developments and Assay Validation. Environ Mol Mutagen 52:681–684.

Dertinger SD, Phonethepswath S, Franklin D, Weller P, Torous DK, Bryce SM, Avlasevich S, Bemis JC, Hyrien O, Palis J, MacGregor JT. 2010. Integration of mutation and chromosomal damage endpoints into 28-day repeat dose toxicology studies. Toxicol Sci 115:401–411.

Dertinger SD, Bryce SM, Phonethepswath S, Avlasevich SL. 2011. When pigs fly: Immunomagnetic separation facilitates rapid determination of *Pig-a* mutant frequency by flow cytometric analysis. Mutat Res 721:163–170.

Dobrovolsky VN, Boctor SY, Twaddle NC, Doerge DR, Bishop ME, Manjanatha MG, Kimoto T, Miura D, Heflich RH, Ferguson SA. 2010a. Flow cytometric detection of *Pig-A* mutant red blood cells using an erythroid-specific antibody: Application of the method for evaluating the in vivo genotoxicity of methylphenidate in adolescent rats. Environ Mol Mutagen 51:138–145.

Dobrovolsky VN, Miura D, Heflich RH, Dertinger SD. 2010b. The in vivo *Pig-a* gene mutation assay, a potential tool for regulatory safety assessment. Environ Mol Mutagen 51:825–835.

Keller P, Payne JL, Tremml G, Greer PA, Gaboli M, Pandolfi PP, Bessler M. 2001. FES-Cre targets phosphatidylinositol glycan class A (PIGA) inactivation to hematopoietic stem cells in the bone marrow. J Exp Med 194:581–589.

Kimoto T, Suzuki K, Kobayashi X-m, Dobrovolsky VN, Heflich RH, Miura D, Kasahara Y. 2011. Manifestation of *Pig-a* mutant bone marrow erythroids and peripheral blood erythrocytes in mice treated with *N*-ethyl-*N*-nitrosourea; Direct sequencing of *Pig-a* cDNA from cells negative for GPI-anchored protein expression. Mutat Res 723:36–42.

Kina T, Ikuta K, Takayama E, Wada K, Majumdar AS, Weissman IL, Katsura Y. 2000. The monoclonal antibody TER-119 recognizes a molecule associated with glycophorin A, specifically marks the late stages of murine erythroid lineage. Br J Haematol 109:280–287.

Miura D, Dobrovolsky VN, Kasahara Y, Katsuura Y, Heflich RH. 2008a. Development of an in vivo gene mutation assay using the endogenous *Pig-A* gene: I. Flow cytometric detection of CD59-negative peripheral red blood cells and CD48-negative spleen T-cells from the rat. Environ Mol Mutagen 49:614–621.

Miura D, Dobrovolsky VN, Mittelstaedt RA, Kasahara Y, Katsuura Y, Heflich RH. 2008b. Development of an in vivo gene mutation assay using the endogenous *Pig-A* gene. II. Selection of *Pig-A* mutant rat spleen T-cells with proaerolysin and sequencing *Pig-A* cDNA from the mutants. Environ Mol Mutagen 49:622–630.

Miura D, Dobrovolsky VN, Kimoto T, Kasahara Y, Heflich RH. 2009. Accumulation and persistence of *Pig-A* mutant peripheral red blood cells following treatment of rats with single and split doses of *N*-ethyl-*N*-nitrosourea. Mutat Res 677:86–92.

Miura D, Shaddock JG, Mittelstaedt RA, Dobrovolsky VN, Kimoto T, Kasahara Y, Heflich RH. 2011. Analysis of mutations in the *Pig-a* gene of spleen T-cells from *N*-ethyl-*N*-nitrosourea-treated Fisher 344 rats. Environ Mol Mutagen 52:419–423.

Offer T, Ho E, Traber MG, Bruno RS, Kuypers FA, Ames BN. 2005. A simple assay for frequency of chromosome breaks and loss